THE ATLANTIC-WIDE RESEARCH PROGRAMME FOR BFT

(GBYP Phase 14)

SHORT-TERM CONTRACT FOR THE AERIAL SURVEY DATA ANALYSIS – TASK B

Preparation of aerial survey data and environmental data to estimate abundance and biomass of Bluefin Tuna in the Mediterranean Sea using model-based analysis

Final Report

December 2025

INSTITUTO ESPAÑOL DE OCEANOGRAFÍA (IEO-CSIC)

D. Alvarez-Berastegui, M. P. Tugores Ferra, D. Ottmann, I. Alvarez, P. Reglero,

CREEM, University of St Andrews

L. Burt, C. G. M. Paxton, M. Chudzińska

Co-funded by the European Union

Please cite this report as Álvarez-Berastegui D, Tugores MP, Burt L, Paxton CGM, Chudzinska M, Ottman D, Alvarez I, Reglero P, (2025). Preparation of aerial survey data and environmental data to estimate abundance and biomass of Bluefin Tuna in the Mediterranean Sea using model-based analysis. Provided to ICCAT, December 2025 (Unpublished).

Document control

Please consider this document as an uncontrolled copy when printed.

Version	Date	Reason for issue	Prepared by	Checked by
1	18 December	First draft	DA, PT, PR	DA, PT
2	19 December	Second draft	DA, PT, PR	DA, PT, PR

Contents

SUMMARY 5

INTRODUCTION 6
1. PREPARATION OF THE AERIAL SURVEY DATA 7
1.1. Methods 7
Aerial survey data, definition of transects and segments 7
Probability of detection 8
1.2. Results 9
Aerial survey data 9
1.3. Discussion 11
2. ENVIRONMENTAL DATA REPOSITORY AND COMBINATION OF AERIAL SURVEY DATA WITH ENVIRONMENTAL DATA 11
2.1. Introduction 11
2.2. Methods 15
2.2.1. Aerial surveys data (2010-2017; 2017-2025) 15
2.2.2. Two scale analytical approach 16
2.2.3. Selection of environmental variables 17
Bathymetry and slope 17
Sea surface temperature 17
Chlorophyll-a 17
Salinity 17
Depth of the mixed layer 18
Fronts and mesoscale activity: spatial gradients of salinity and sea surface temperature . 18
Temporal increase of sea surface temperature 18
2.2.4. Data extraction and creation of a local repository 19
Primary environmental data and data sources 19
Derived environmental data 19
Computation of derived environmental data 20
2.2.5. Area-based environmental analysis 25
2.2.6. Aerial-survey segment-based environmental analysis 25

2.3. Results 27
2.3.1. Environmental variability within the BFT reproductive area 27
2.3.2. Environmental variability within aerial survey segments 43
Multidimensional analysis 50
2.4. Discussion 51
2.5. Conclusions and considerations for the future standardization of abundance indices from aerial surveys 53
ACKNOWLEDGEMENTS 54
REFERENCES 55
Appendix A. Summary of school sizes, biomass and perpendicular distances by year 59
Appendix B. Calculating perpendicular distance 60
Appendix C. Detection function selection 61
Appendix D. Spatio-temporal variability in sea surface temperature (SST) across the aerial survey timeframe (28 May–11 July) from 2010 to 2025 62
Appendix E. Spatio-temporal variability in sea surface chlorophyll-a (CHL) across the aerial survey timeframe (28 May–11 July) from 2010 to 2025 63
Appendix F. Spatio-temporal variability in sea surface salinity (SSS) across the aerial survey timeframe (28 May–11 July) from 2010 to 2025 64
Appendix G. Spatio-temporal variability in sea surface mixed layer depth (MLD) across the aerial survey timeframe (28 May–11 July) from 2010 to 2025 65
Appendix H. Spatio-temporal variability in spatial gradient of sea surface temperature (GradSpat SST) across the aerial survey timeframe (28 May–11 July) from 2010 to 2025 66
Appendix E. Spatio-temporal variability in spatial gradient of sea surface salinity (GradSpat SSS) across the aerial survey timeframe (28 May–11 July) from 2010 to 2025 67

SUMMARY

This report is the deliverable of the CALL FOR TENDERS – AERIAL SURVEY FOR BLUEFIN SPAWNING AGGREGATIONS: 2025 AERIAL SURVEY DATA ANALYSIS AND FURTHER DEVELOPMENT OF MODEL-BASED APPROACHES FOR THE STANDARDIZATION OF THE INDEX OF ABUNDANCE – ATLANTIC-WIDE RESEARCH PROGRAMME FOR BLUEFIN TUNA (ICCAT GBYP – PHASE 14) (ICCAT GBYP CIRCULAR # G-00510/2025 on 26 August 2025). The objective of this deliverable is to prepare and harmonise aerial survey data and the environmental information required for the future model-based estimation of the abundance and biomass of the Atlantic Bluefin tuna (*Thunnus thynnus*) spawning stock in the Mediterranean Sea. The work has been conducted jointly by IEO-CSIC and CREEM (University of St Andrews), integrating expertise in operational oceanography, fisheries ecology and statistical analysis.

The study is structured around four main components: (i) preparation and standardisation of aerial survey data collected in the Balearic Sea for the period 2017–2025; (ii) compilation and organisation of a structured repository of environmental variables for the period 2010-2025 (providing the flexibility to include earlier aerial surveys if required); (iii) integration of aerial observation data with environmental information at spatial scales relevant to the analysis of Atlantic Bluefin tuna spawning aggregations; and (iv) comprehensive assessment of the effective environmental variability within the sampling areas and along the transects surveyed during the aerial campaigns.

The environmental analysis follows a multiscale approach. It combines the characterisation of inter-annual variability in key environmental variables during the survey time window with an assessment of the effective environmental heterogeneity experienced at the scale of the sampled flight segments. The variables considered include sea surface temperature, salinity, chlorophyll-a concentration, mixed layer depth, and metrics describing frontal systems and spatial gradients. The results reveal a clear inter-annual environmental structure. This structure is characterised by shifts in the position of frontal systems associated with the confluence of recent Atlantic and resident Atlantic waters. In addition, a progressive advance is observed in the timing at which the 20 °C thermal threshold linked to the onset of reproduction is reached.

Multivariate analyses indicate that surveys conducted in different years take place under partially differentiated environmental conditions. This suggests that a substantial proportion of the variability observed in abundance indices derived from aerial surveys may be driven by changes in the accessibility and spatial distribution of spawning habitat. These changes may therefore reflect environmental modulation of detectability rather than true fluctuations in spawning biomass. This finding supports the need to move towards habitat-explicit standardisation models. Such approaches are consistent with developments promoted by ICCAT within the framework of the Management Strategy Evaluation.

Overall, the report provides a robust and reproducible methodological basis for integrating environmental information into the future standardisation of abundance indices derived from

GBYP aerial surveys. This integration is expected to improve the robustness, comparability, and interpretation of the indicators used in the assessment and management of Atlantic Bluefin tuna.

INTRODUCTION

Aerial surveys have been undertaken in Mediterranean Sea to detect Atlantic Bluefin tuna (BFT) between 2010 and 2025 under the auspices of the International Commission of the Conservation of Atlantic Tunas (ICCAT), within the framework of the Atlantic-wide Research Programme for Bluefin Tuna (GBYP). The main objectives of the GBYP are to improve understanding of key biological and ecological processes, enhance current stock assessment methodologies, strengthen management procedures and support scientific advice.

This report responds to Task B as specified in the call for tender ICCAT GBYP Circular No. G-00510/2025. It presents a detailed description of the data processing steps undertaken in preparation for analyses aimed at estimating spawning stock biomass using model-based approaches endorsed by the BFT Working Group.

The task comprises three main components. These include the preparation and standarisation of aerial survey data, the development of a repository of environmental data covering the spatial and temporal extent of the surveys, and the integration of both datasets into a unified analytical framework.

The document is structured into two main sections. The first section, 1. Preparation of the aerial survey data, describes the procedures applied to the processing and standardisation of the aerial survey information (for years 2017-2025). The second section, 2. Environmental data repository and combination of aerial survey data with environmental data, addresses the development of the environmental data repository, the extraction of environmental information on the aerial survey samples and the analyses of environmental variability parameters relevant for the standardization of abundance indices.

1. PREPARATION OF THE AERIAL SURVEY DATA

1.1. Methods

Aerial survey data, definition of transects and segments

The aerial surveys are designed using distance sampling methodology (Buckland *et al.,* 2001). A plane flies along a series of parallel transects (placed with a random start point) and observers search for BFT. On detection of a school (of one or more fish), observers record key information (such as school size, total weight of the school and angle of declination).

For the model-based analysis, the data are required to be in the form of **segments** of search effort along **flight transects**. Therefore, segments are defined as subunits of specific distance of the transects. The number of individual fish (for example) detected in a segment will form the response in the model with relevant environmental variables as explanatory variables in the model.

The survey data collected during the aerial surveys in the Balearic Sea (block A) was provided by ICCAT GBYP.

The target length of segments was 20 km; however, some segments may be shorter because of natural breaks in search effort (such as going off the transect to confirm the sightings). Some segments may be up to 30 km to avoid splitting a section into lengths much smaller than 20 km.

Estimates of size (individual fish) and biomass (total weight) of a school recorded by the professional observers were used unless these were missing, in which case, estimates from the scientific observers were used. Where estimates from both observers were missing for a detected school (or perpendicular distance was missing), the median value recorded for that year was used (see Appendix A). These median values were calculated before any schools were excluded (see below). The median values were used rather than the average because the distributions were right skewed and so the average can be inflated by large values.

Schools were included in the data processing if they were:

- adult schools (schools identified as 100% small schools (fish <25 kg) were excluded),
- detected when on search effort along the transect (and so schools seen when in transit or confirming a previous sighting were not included)
- within 1,500m of the transect.

The truncation distance of 1,500m has been used in previous distance sampling analyses and although this results in a long tail (see later), truncating further would increase the number of segments with no detections.

Three response values were obtained for each segment:

- number of detected schools,
- total number of individual fish, and
- total biomass.

These response values were adjusted for the estimated probability of detection so that, for example, the total number of individual fish for segment *i*, $\widehat{N}_i$, was obtained from

$$\widehat{N}_i = \sum_{j=1}^{J} \frac{s_{ij}}{\hat{p}_{ij}}$$

where for segment *i*, s_{ij} is the size for school *j* (where *J* is the total number of schools in segment *i*) and $\hat{p}_{ij}$ is the estimated probability of detection for school *j*. This is to adjust for missing and underestimated schools (see below).

Probability of detection

Two critical assumptions of distance sampling methods (Buckland *et al*. 2001) are that all schools on the transect (i.e., at zero perpendicular distance) are detected with certainty and that distances are measured without error. Given these assumptions, the distribution of perpendicular distances was used to model how the probability of detection decreases with increasing distance from the transect. The calculation of the perpendicular distances is shown in Appendix B.

Two forms of the detection function were used, a half-normal and hazard rate. In conventional distance sampling, perpendicular distance is the only explanatory variable, but the method can be extended to include additional explanatory variables which affect detectability, such as school size (Marques *et al*. 2007). The variables considered here were:

- year (a factor with 8 levels),
- company (a factor with 3 levels; Airmed, Air Perigord and Action Air),
- logarithm of school size, and
- logarithm of biomass.

The logarithms of the latter two variables were taken to scale down the few very large values recorded (Appendix A). The model with the lowest AIC was selected.

The detection function was fitted in R (R Core Team 2024) using the mrds package (Laake *et al*., 2022).

1.2. Results

Aerial survey data

Over eight years of aerial surveys in block A, a total of 45,357 km of search effort along the transect lines were included. The average length of the created segments was 14.3 km (with a range from 0.1 to 30 km).

The number of detected schools included was 113. A half-normal detection function that included the logarithm of school size was selected (Figure 1.1, Appendix C). The average probability of detection of a BFT school was 0.28 (CV=0.11) (Figure 1.1).

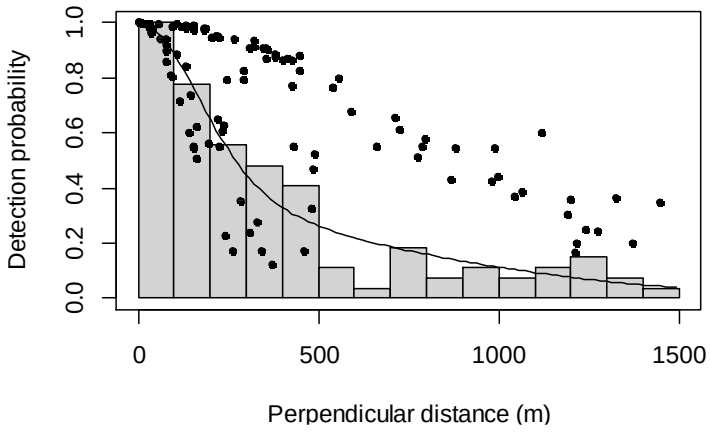

Figure 1.1. Detection function (line) averaged over all school sizes overlaid onto a scaled histogram of perpendicular distances: the dots indicate individual detections.

The location of segments and detected school is shown in Figure 1.2. There were 106 segments which contained detections out of a total of 3,169 segments (3.3%).

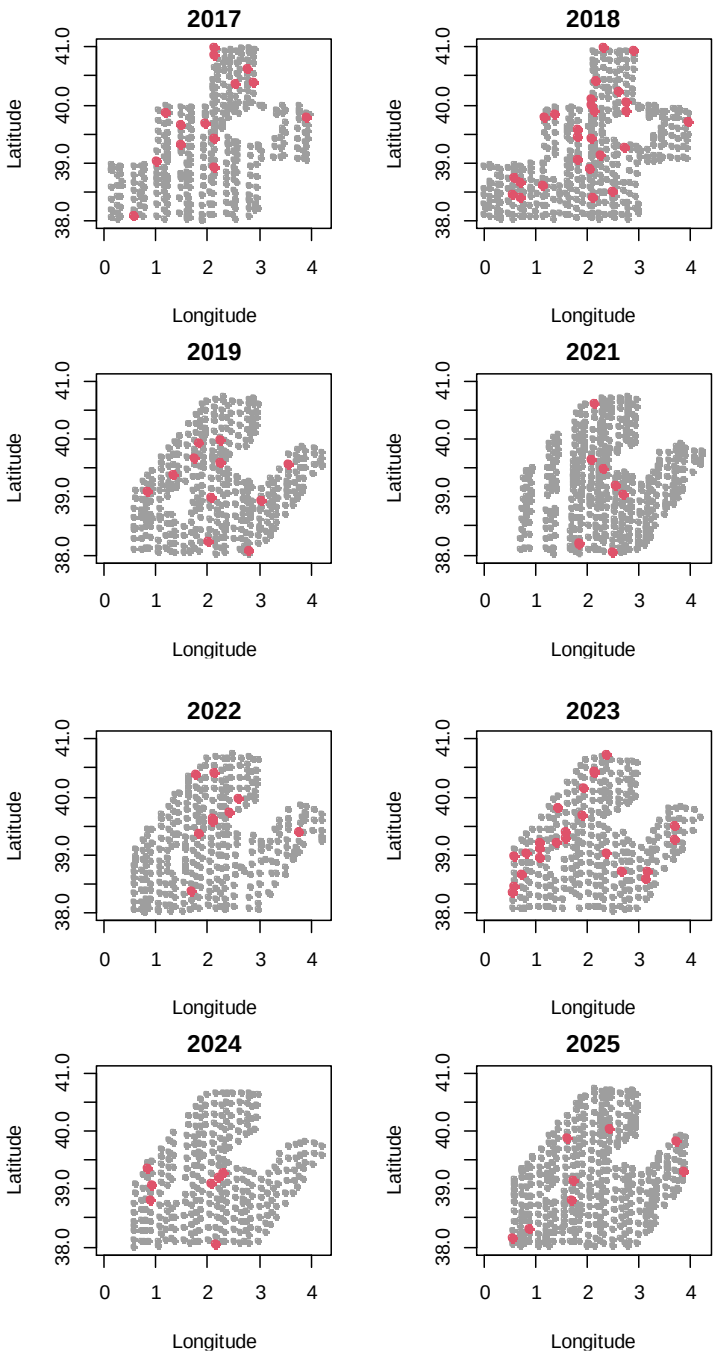

Figure 1.2. Location of mid-point of effort segments (grey dots) and segments where schools of BFT were detected (larger red dots).

1.3. Discussion

The number of schools, fish and total biomass detected in a segment has been obtained. These values have been adjusted for the probability of detection. This detection probability assumes that detection on the transect is certain (i.e. $g(0)=1$), if this is not a valid assumption, the number of schools will be underestimated. In addition, the availability of schools on the transect to be detected has not been considered.

2. ENVIRONMENTAL DATA REPOSITORY AND COMBINATION OF AERIAL SURVEY DATA WITH ENVIRONMENTAL DATA

2.1. Introduction

Reliable estimation of spawning stock biomass (SSB) is one of the fundamental pillars of scientific advice for Bluefin tuna (*Thunnus thynnus*) management. Aerial surveys conducted under the Atlantic-Wide Research Programme for Bluefin Tuna (GBYP) of the International Commission for the Conservation of Atlantic Tunas (ICCAT) have become one of the main sources of independent fisheries information on the abundance and spatial distribution of adult spawners during the spawning period (ICCAT, 2011; Walter *et al.* 2025).

The Balearic Sea represents one of the most important and persistent breeding areas for the eastern stock of Atlantic Bluefin tuna, as demonstrated by larval studies, direct observations of adult aggregations, and integrated physical and biological oceanographic analyses (Alemany *et al.,* 2010; Reglero *et al.,* 2012). Consequently, abundance indices derived from aerial surveys in this region play a particularly critical role in stock assessment processes and in the Management Strategy Evaluation (MSE) framework adopted by ICCAT (i.e. ICCAT, 2021).

In the context of MSE, the quality, stability and interpretability of abundance indices directly influence the robustness of operational models and the performance of catch control rules under different uncertainty scenarios (Walter *et al.* 2025). Therefore, understanding the physical and environmental mechanisms that condition the spatial-temporal distribution of spawners is essential to ensure that indices reflect actual changes in spawning biomass and not indirect responses to oceanographic variability.

Need for adequate spatial and temporal coverage of reproductive aggregations

The reliability of abundance estimates obtained from aerial surveys depends on the sampling design adequately covering the period and geographical area where reproductive aggregations occur. In the western Mediterranean, Bluefin tuna aggregate near the surface for a relatively short period of time, generally between late May and early July (García *et al.,* 2005; Gordoa and Carreras, 2014).

The start of spawning is closely linked to temperature thresholds of around 19–20 °C, while peak reproductive activity is concentrated around the summer solstice (Gordoa and Carreras, 2014). However, the spatial location of reproductive aggregations is not fixed, but rather responds to the distribution of suitable oceanographic habitat, which can vary significantly from year to year. As a result, small differences in the sampling schedule or spatial coverage of flights can lead to substantial variations in encounter rates, regardless of actual changes in stock abundance.

The spatial-temporal distribution of the Bluefin tuna breeding habitat in the Balearic Sea is strongly influenced by surface circulation and the position of fronts associated with the confluence of recent Atlantic waters and resident Mediterranean waters. Numerous studies have

shown that spawning areas are preferentially associated with these saline fronts, as well as with regions characterised by temporal gradients in surface temperature (temperature jumps above 20 degrees) and mesoscale activity compatible with larval retention processes (Alemany *et al.,* 2010; Reglero *et al.,* 2012; Álvarez-Berastegui *et al.,* 2014, 2016).

In this context, the inter-annual variability of surface circulation in the Balearic Islands emerges as a key factor in understanding the changes observed in the distribution of pelagic species. Previous studies have shown that the position of the saline front at the beginning of summer depends on the presence or absence of Western Intermediate Water (WIW) in the Ibiza and Majorca channels, which is in turn controlled by winter atmospheric forcing in the north-western Mediterranean (Balbín *et al.,* 2014).

A recent study delves into the inter-annual variability of oceanography and shows how changes in surface circulation can cause a systematic northward shift of the saline front during the sampling period, substantially modifying the structure of the pelagic habitat in the Balearic Sea (Camps 2025). This shift has direct implications for the distribution of pelagic species, including large predators such as Bluefin tuna, whose reproductive aggregation patterns are closely linked to the position of these fronts. In years characterised by a more northerly penetration of recent Atlantic waters, the salt front may shift to higher latitudes, redistributing the potential reproductive habitat outside the areas traditionally sampled or altering its overlap with flight transects. This mechanism provides a coherent physical explanation for part of the inter-annual variability observed in abundance indices derived from aerial surveys, even in scenarios where no significant variation in spawning biomass is expected.

In addition to the variability induced by shifts in salt fronts and surface circulation, marine heat waves (MHWs) represent another type of physical forcing that can have significant effects on the distribution and reproductive phenology of pelagic organisms, including Bluefin tuna. MHWs are abnormally high sea surface temperature events that persist for days or weeks and have been increasing in both frequency and intensity in the Mediterranean in recent decades in response to global warming and regional climate variability (Juza *et al.,* 2021; Rosselló *et al.,* 2023).

These extreme thermal events can modify the thermal conditions associated with reproductive physiology, migration and spawning behaviour in species sensitive to thermal thresholds, shifting or condensing the reproductive period within the spawning season (Gordoa and Carreras, 2014). In tuna and other pelagic species, abnormal temperature conditions can advance or delay reproductive phenology, affect the synchronization between reproductive aggregations and oceanographic conditions favourable for successful spawning, and thus alter the interpretation of abundance indices that assume a relatively fixed reproductive season. On the other hand, the increase in temperature being detected in the study area also affects the stratification of the surface layers of the sea, potentially increasing the depth of the mixing layer and the possible vertical distribution of adult individuals, which could have effects on the detectability of schools and their abundance from the aircraft.

Implications for the standardisation of abundance indices and methodological transition in the context of GBYP aerial surveys

From the early stages of the GBYP programme to the present day, abundance indices have been estimated using a design-based approach, based on distance sampling using linear transects (Buckland *et al.,* 2001). Although this approach has made it possible to generate a time series applicable to the assessment process (Walter *et al.* 2025), it implicitly assumes that the spatial distribution of breeders is stationary with respect to the sampling design, an assumption that is difficult to sustain in a system as dynamic as the Balearic Sea.

To address these limitations, the GBYP has promoted the development of an approach based on spatially explicit models, in which the density of spawners is modelled as a function of relevant environmental variables. Analyses conducted during Phase 12 of the GBYP have shown that oceanographic variables related to frontal structure and surface circulation are significantly related to observed abundance (Paxton *et al.,* 2023). Shifts in the salt front and relevant changes in temperature (Camps 2025, Juza *et al.* 2022) substantially reinforce this methodological transition, demonstrating that inter-annual variability in surface circulation and salt front displacement must be explicitly considered in the standardisation of abundance indices. Ignoring these processes can lead to interpreting what are actually spatial responses of the spawning stock to a highly variable physical environment as population changes.

Advancing towards a robust model-based abundance estimation methodology requires detailed characterisation of environmental variability at multiple scales. On the one hand, it is necessary to analyse inter-annual variability across the entire study area and sampling period in order to identify years with contrasting oceanographic configurations. On the other hand, it is essential to assess environmental variability at the specific sampling scale, as relatively small changes in dates or areas covered can introduce systematic differences in the environmental conditions observed.

The integration of both levels of analysis allows us to assess the extent to which inter-annual differences in abundance indices can be attributed to shifts in spawning habitat associated with surface circulation and frontal dynamics, rather than to actual changes in spawning stock biomass. This approach is an essential preliminary step in the development of standardised abundance indices that are robust and fully consistent with their use in stock assessment processes and within the framework of ICCAT's MSE, in full alignment with the objectives of Task B of the GBYP call.

Considering the different aspects described above—including inter-annual variability in surface circulation, displacement of the saline front, the occurrence of extreme thermal events and their potential influence on the distribution and reproductive phenology of Bluefin tuna— this document presents an integrated analysis of environmental variability in the Balearic Sea spawning area during the GBYP aerial survey sampling period. The study is based on the selection and characterisation of the study area, the use of aerial survey data corresponding to the periods 2010–2017 and 2017–2025, and the application of a methodological approach aimed at assessing

environmental variability both at the scale of the spawning area and at the scale of effective sampling.

The environmental variables considered have been selected from previous studies that have demonstrated their relevance to the location and dynamics of the Bluefin tuna breeding habitat in the western Mediterranean. The data required for their calculation have been obtained from multiple sources and observation platforms, including coastal observation systems (e.g. coastal radar), satellite environmental remote sensing products and numerical oceanographic model outputs, all of which are publicly available. From these datasets, additional variables have been derived that are specifically designed to monitor oceanographic processes known to be relevant to Bluefin tuna, such as the location of fronts and mesoscale activity, thus providing a coherent framework for the analysis of temporal and spatial variability.

Objectives

In this context, the overall objective of the present study is to characterise environmental variability in the study area during the Bluefin tuna spawning period, with particular emphasis on the spatial scales relevant to the aerial observation of spawning aggregations, and to provide quantitative environmental information to support the future habitat-based standardisation of abundance indices derived from aerial surveys. Specifically, the operational objectives are to:

i. Construct an environmental data repository based on public data sources and process new environmental information relevant to the study of Bluefin tuna reproductive ecology, covering the periods 2010–2015 and 2016–2025.

ii. Analyse the spatio-temporal variability of a set of key environmental variables in the study area during GBYP survey periods *(note that, although these periods were addressed as separate subtasks in the contract, they are analysed jointly here to improve the interpretation of the time series)*.

iii. Extract and explore environmental variables at the centres of the sub-transects defined from the flight transects, providing a quantitative and methodological basis to inform and support future abundance index standardisation exercises, which will be developed in subsequent projects using dedicated model-based approaches.

2.2. Methods

2.2.1. Aerial surveys data (2010-2017; 2017-2025)

Identification of transects, segments and survey dates

Here we define "transects" as the flight units defined by the data provided by GBYP and converted into continuous lines by CREEMS (data used for this analysis was the processed before 2025/12/17). From these transects, sub-units referred to as "segments" have been created, corresponding to 20-km elements within each transect. This distance has been selected based on studies conducted at the IEO to characterise the scale of the Rossby radius in the area, which indicates spatial scales of 10–50 km for mesoscale processes and 5–15 km for submesoscale processes. This has been historically applied in the study area for the analysis of environmental variability related to tuna ecology (see Alemany *et al.*, 2010 for more information).

This distance might be modified when statistically analysing tuna abundances, increasing the segment length if required in order to reduce the number of zeros in the distributions. This aspect will need to be assessed when examining the distribution of abundances by segments in future studies aimed at the standardisation of abundance indices. The systems used to define the location of the segments are implemented in R and are available for application. Survey dates have been collected in Table 2.1.

Table 2.1. Summary of survey dates by year.

Year	Dates
2010	01 June – 02 July
2011	15 June – 11 July
2013	06 June – 06 July
2015	01 June – 11 July
2017	30 May – 26 June
2018	31 May – 28 June
2019	28 May – 28 June
2022	07 June – 27 June
2023	01 June – 26 June
2024	04 June – 24 June
2025	09 June – 26 June

2.2.2. Two scale analytical approach

The analysis of the environmental variables was conducted following two approaches. First, an area-based analysis was conducted for the area and temporal window of the aerial survey samplings (see Figure 2.1). This analysis has the objective of providing information for understanding the environmental variability in the region comparably among years. Second, the environmental variability at the identified segments will inform specific aspects of the sampling program.

Regarding the area-based analysis, the time window encompasses from 28 March to 11 July between the years 2010 and 2025. The study area was the one that was recurrently covered by the aerial surveys (Figure 2.1). For the delineation of the study area, all points contained in the effort file provided by the GBYP were plotted on a map, and a buffer area of approximately 0.25 degrees was defined. Figure 2.1 shows the location of this area and the position of the sampling points. It should be noted that, for this analysis, the quadrant without transects north of Menorca was also included, as the objective is to analyse general changes affecting the entire area. The analysis at the segments consisted of the extraction of environmental variables in the surroundings of the MidLon, MidLat of each location (further explained in subsequent sections).

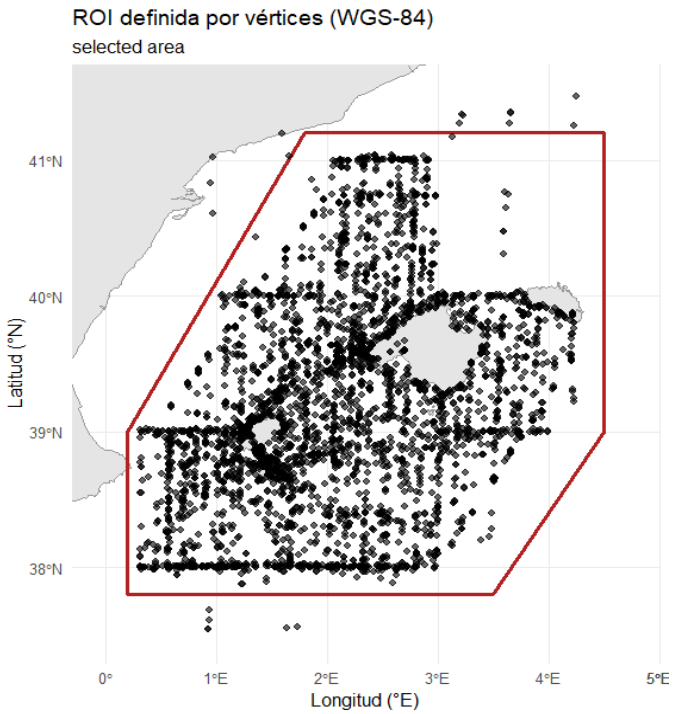

Figure 2.1. Map showing the study area where aerial surveys have been conducted. The red line is the polygon on which area-based analysis is performed.

2.2.3. Selection of environmental variables

Environmental variables were selected according to their potential explanatory power on Bluefin tuna presence, abundance or detectability, based on previous knowledge.

Bathymetry and slope

In the western Mediterranean, BFT spawning areas have been identified at bottom depths ranging from 1250 and 2250 m (Alemany *et al.,* 2010). In the Gulf of Mexico spawning occurs at wider ranges of bottom depths, including the shelf break, the slope and the deeper waters (Hazen *et al.,* 2016), with hotspots occurring in the shelf slope (Block *et al.,* 2005). Bottom topography influences ocean circulation from mesoscale to large-scale (Solodoch, 2020; Gille *et al.,* 2003; Marshall, 1995). BFT spawns at the sea surface influenced by ocean currents, either bathymetry or slope, likely exert direct effects on these currents and may affect the estimates derived from the aerial surveys.

Sea surface temperature

The influence of sea surface temperature (SST) on the timing and spatial distribution of BFT spawning is well established (García *et al.,* 2005; Alemany *et al.,* 2010; Koched *et al.,* 2013; Reglero *et al.,* 2014). Reproductive activity begins when SST reaches 19–20ºC (Muhling *et al.,* 2013), and SST also triggers gonadal development in mature individuals arriving in Balearic waters (Medina *et al.,* 2002). Higher SST enhances embryo and larval growth and survival by reducing developmental time (Gordoa and Carreras, 2014), with larvae preferring 23–28ºC (Muhling *et al.,* 2013). Juveniles show a similar thermal preference (24–27ºC) but inhabit waters between 20–28ºC (Trueman *et al.,* 2023), spending most of their time below 28ºC with brief excursions to cooler or slightly warmer waters (Marcek *et al.,* 2016). Adults of congeneric species avoid surface waters by diving deeper when temperatures exceed ~24–26ºC (Fujioka *et al.,* 2021, 2025).

Chlorophyll-a

Several studies have shown that BFT spawning grounds are located in low sea surface chlorophyll-a concentration areas (Muhling *et al.*, 2011; Koched *et al.,* 2013; Muhling *et al.,* 2013; Llopiz and Hobday, 2015). It has been hypothesised that this could be a strategy of adults to avoid spawning in areas with high abundance of predators (Ottman *et al.,* 2021). On the other hand, in the Balearic waters Atlantic (less saline) and Mediterranean waters (more saline) meet. Although they also display different SST, the seasonal sea warming makes it very difficult, if not impossible, to detect the frontal area with the aid of SST. As Mediterranean waters are less productive, CHL could also be used to provide complementary information regarding the position of the front, up to some extent (Alvarez-Berastegui *et al.,* 2016).

Salinity

In the western Mediterranean, the oceanic front formed in the confluence of recently advected Atlantic waters (lower saline) and resident Mediterranean waters (higher saline) can be identified by means of sea surface salinity (SSS), with the front generally showing values of 37.5 psu (Balbín

et al., 2014). Fronts have been found to be important spawning grounds for many marine species, including BFT (Bakun, 2006; Cornic and Rooker, 2018; Suthers *et al.,* 2023), probably due to retention eddies and filaments observed in these areas (Alvarez-Berastegui *et al.,* 2016). On the other hand, the distribution of yolk sac BFT larvae in several spawning grounds have been found to have strong relationships with SSS, indicating that this variable is one of the most relevant environmental variables for identifying specific spawning locations (Alemany *et al.,* 2010, Reglero *et al.,* 2012, Koched *et al.,* 2013, Muhling *et al.,* 2010, 2013). In the Balearic Island, BFT larvae seemingly prefer salinity between 36.9 and 37.7 (Alemany *et al.,* 2010).

Depth of the mixed layer

One open question for improving the standardization of abundance indices is the potential effect of the mixed layer depth on the vertical distribution of the adult individuals. On one hand, increase of temperature in the surface layers seems to increase probability of adult aggregations (Di Natale *et al.,* 2015), but high temperatures in the surface may also affect the vertical distribution of adults, which could avoid extreme temperatures by lowering their location in the water column, affecting detectability. These effects can be explored if adequate indicators are integrated in the analysis. Therefore, we extracted the mixed layer depth (MLD) from hydrodynamic models to explore spatial and inter-annual variability.

Fronts and mesoscale activity: spatial gradients of salinity and sea surface temperature

As noted in the previous sections, the spawning ecology of BFT is linked to mesoscale activity associated with the main fronts during the spawning season. Sea surface salinity is a good proxy for identifying water masses and frontal areas, but another variable that provide better identification of the precise location of the front is the spatial gradients of the surface salinity field, especially when included in spatial models as interaction effect with salinity (Alvarez-Berastegui *et al.* 2014). Hence, the spatial gradients SSS were considered as key environmental variables within this study. Sea surface temperature front have been also computed, however, it has to be borne in mind that in the Mediterranean SST fronts generally weaken or disappear during the summer period, and influence on abundances may be less relevant.

Temporal increase of sea surface temperature

Sustained increase in sea surface temperature set the onset of the spawning activity for yellowfin tuna (Margulies *et al.,* 2007), and a similar pattern could apply to Bluefin tuna (Heinisch *et al.,* 2008). In the Balearic Islands, the temporal gradient of SST over the preceding fifteen days has proven to be related to predict BFT spawning grounds. Because water temperature rises rapidly in early summer in the Balearic Islands, SST gradients over both 15-day and 7-day periods were evaluated (Álvarez Berastegui *et al.,* 2016).

2.2.4. Data extraction and creation of a local repository

Environmental variables consisted in a set of primary environmental variables downloaded from freely available datasets and derived variables, which were calculated from the primary, derived variables. Both sets of variables were incorporated in a **structured data repository** within a local server.

Primary environmental data and data sources

Environmental data were downloaded from three free on-line data sources: i) the EMODNET database for bathymetry, ii) the Copernicus Marine Service for satellite and hydrodynamic models, and iii) the SOCIB Data Repository for current data in the Ibiza Channel from HFR radar (Note that the HFR radar only covers part of the study area in the Ibiza channel). Downloaded variables consisted of bathymetry (Depth), sea surface temperature (SST), sea surface chlorophyll-a (CHL), sea surface salinity (SSS), depth of the mixed layer (MLD) and current intensity in the x and y directions (U, V), see Table 2.2 for a complete list. These data were downloaded at the best available spatial resolution in NetCDF format, using direct download from https connections to web servers for EMODNET data, through Copernicus Marine Toolbox or through http thredds services for SOCIB data. Downloaded variables were stored in the **structured data repository**, with different directories mirroring the data sources. A complete list of downloaded variables, including their spatial domain, resolution, and source datasets, is provided in Table 2.2.

Derived environmental data

In order to depict the spatial gradients of bottom depth, temperature, and salinity, as well as the temporal increase of temperature the following variables were used: slope, spatial gradient of SST (GradSpat_SST), spatial gradient of SSS (GradSpat_SSS), 7-day SST increase (SST7dinc), 15-day SST increase (SST15dinc) and 7-day CHL average (CHL_7dL3). The variables reflecting the temporal increase of SST (7d_incSST and 15d_incSST) were only calculated for the segments analysis, but not for the area-based analysis. These metrics quantify short-term thermal variability and require a daily time series. Segments are calculated for individual points at clearly defined sampling dates, thus enabling the estimation of such metrics. However, in the context of the area-based analysis, derived from a 45-day composite (28/05 - 11/07), the temporal resolution required to calculate lag-based thermal anomalies is not preserved and temporally lagged products would be methodologically inconsistent.

Derived variables were computed from the environmental datasets obtained from the sources described above. Each variable was processed at the highest spatial resolution permitted by the original data, ensuring that no additional spatial aggregation was introduced during derivation. The resulting products were archived in NetCDF format, in a **structured data repository**, with different spatial domains and resolution, according to the originating variable from which they were computed. A detailed description of all derived variables, including their spatial domain, resolution, and source datasets, is provided in Table 2.3.

Computation of derived environmental data

Data extraction and calculation of derived variables was developed in R language (R Core Team, 2023), using the following packages: ncdf4 (Pierce and Pierce, 2019), terra (Hijmans, 2023b), raster (Hijmans, 2023a) and sf (Pebesma and Bivand, 2023). The variables computed were the following:

Slope

The slope was calculated from downloaded EMODNET bathymetry using the function 'terrain' from the raster package (Hijmans, 2023a). The function was applied using the method described by Horn (1981), which computes slope considering the 8 neighbouring cells from the target cell. This is better suited for rough surfaces like those observed at the continental slope. We include a Figure 2.showing the bathymetry downloaded data (Figure 2.3A) and the derived slope (Figure 2.3B).

Spatial gradients

The spatial gradients of SST and SSS were computed using a second-order central difference scheme. This is a standard numerical method for spatial gradient calculation (Burden & Faires, 2011; Gonzalez & Woods, 2018).

For each grid cell, the partial derivatives in the east-west ($\frac{\partial z}{\partial x}$) and north-south directions ($\frac{\partial z}{\partial y}$) are estimated from the four orthogonal neighbouring cells, divided by twice the grid spacing (Eq. 1 and 2, respectively). The magnitude of the spatial gradient of the variable Z (Z_{spg}) was then obtained as the Euclidean norm of the two components (Eq. 3). The equations read as follows:

$$\frac{\partial z}{\partial x} = \frac{z_{x_1} - z_{x_2}}{2\, r_x} \quad \text{(Eq. 1)}$$

$$\frac{\partial z}{\partial y} = \frac{z_{y_1} - z_{y_2}}{2\, r_y} \quad \text{(Eq. 2)}$$

$$Z_{spg} = \sqrt{\left(\frac{\partial z}{\partial x}\right)^2 + \left(\frac{\partial z}{\partial y}\right)^2} \quad \text{(Eq. 3)}$$

where $\frac{\partial z}{\partial x}$ and $\frac{\partial z}{\partial y}$ are the partial derivatives of the variable *Z* in the x and y direction, respectively, and r_x and r_y are the spatial resolution of the pixels.

Short temporal variability

Variables indicating short temporal variability were also computed, in particular, 7-day and 15-day temperature increments and 7-day CHL average. Temporal increments for sea surface temperature at 7-day and 15-day lags were computed as the difference of temperature at each grid cell between the sampling date and the previous 7 and 15 days, respectively, following Álvarez-Berastegui *et al.,* 2016.

$$T_{SS\Delta t\_inc} = T_{SStk} - T_{SS\Delta tk} \quad \text{(Eq. 4)}$$

The 7-day average of sea surface chlorophyll-a, computed as the average CHL for 7 days previous to each sampling date.

Day exceeding a temperature threshold

The day of the year at which SST exceeded the 20ºC threshold suggesting the start of the BFT reproductive season in the area was also computed. For this, data was transformed into day of the year using the package 'lubridate' (Gromelund and Wickman, 2011). For this, descriptive statistics reflecting the minimum, maximum, mean and SD of temperature for each year in the period 2010-2025 were computed for the area covered by the aerial survey (see Figure 2.1). The amount of grid cells that were above the selected temperature threshold were also computed.

Table 2.2. Environmental variables downloaded from free sources: variable name, acronym, type of data, product name, spatial resolution (º: decimal degrees; Km: kilometers), temporal scale, spatial domain, and data sources.

Variable	Acronym (units)	Type of data	Product name	Spatial resolution	Temporal scale	Spatial domain	Institution	DOI	Reference
Bathymetry	Depth (m)	Digital Terrain Model	EMODnet Bathymetry DTM 2024 Release	0.001º	-	Longitude: -6.032292, 42.35521 Latitude: 30.06771, 47.37604	European Commission	https://doi.org/10.12770/cf51df64-56f9-4a99-b1aa-36b8d7b743a1	https://emodnet.ec.europa.eu/en/bathymetry
Sea surface temperature	SST (ºC)	Satellite	SST_MED_SST_L4_REP_OBSERVATIONS_010_021	0.05º	daily	Longitude: -18.15002, 36.35002 Latitude: 30.09992, 46.05008	Copernicus	https://doi.org/10.48670/moi-00173	Pisano *et al.*, 2016
Sea surface chlorophyll	CHL (mg m^{-3})	Satellite	OCEANCOLOUR_MED_BGC_L4_MY_009_144	1 Km	daily	Longitude: -6, 36.5 Latitude: 30, 46	Copernicus	https://doi.org/10.48670/moi-00300	Volpe *et al.*, 2019
Sea surface salinity	SSS (-)	Model	MEDSEA_MULTIYEAR_PHY_006_004	0.042°	daily	Longitude: -6.020833, 36.3125 Latitude: 30.16667, 46	Copernicus	https://doi.org/10.25423/CMCC/MEDSEA_MULTIYEAR_PHY_006_004_E3R1	Escudier *et al.*, 2020
			MEDSEA_ANALYSISFORECAST_PHY_006_013	0.042°	daily	Longitude: -17.3125, 36.3125 Latitude: 30.16667, 46	Copernicus	https://doi.org/10.25423/CMCC/MEDSEA_ANALYSISFORECAST_PHY_006_013_EAS8	Clementi *et al.*, 2021
Mixed layer depth	MLD (m)	Model	MEDSEA_MULTIYEAR_PHY_006_004	0.042°	daily	Longitude: -6.020833, 36.3125 Latitude: 30.16667, 46	Copernicus	https://doi.org/10.25423/CMCC/MEDSEA_MULTIYEAR_PHY_006_004_E3R1	Escudier *et al.*, 2020
			MEDSEA_ANALYSISFORECAST_PHY_006_013	0.042°	daily	Longitude: -17.3125, 36.3125 Latitude: 30.16667, 46	Copernicus	https://doi.org/10.25423/CMCC/MEDSEA_ANALYSISFORECAST_PHY_006_013_EAS8	Clementi *et al.*, 2021
Current intensity	Cur (m s^{-1})	Observational	hf_radar_ibiza-scb_codarssproc001	3 Km	hourly	Ibiza Channel (80 Km area)	SOCIB	https://doi.org/10.25704/17GS-2B59	Tintoré *et al.*, 2020

Table 2.3. Environmental variables derived from the downloaded products: variable name, acronym and units, originating variable (or variable from which the variable is derived), spatial resolution (º: decimal degrees; Km: kilometers) and temporal resolution.

Variable	Acronym (units)	Originating variable	Spatial resolution	Temporal scale	Spatial domain	Institution
Slope	slope (degrees)	Bathy	0.001º	-	Longitude: -6.032292, 42.35521 Latitude: 30.06771, 47.37604	COB-IEO
Spatial gradient of sea surface temperature	GradSpat_SST (ºC)	SST	0.05º	daily	Longitude: -18.15002, 36.35002 Latitude: 30.09992, 46.05008	COB-IEO
Spatial gradient of sea surface salinity	GradSpat_SSS (mg m-3)	SSS	1 Km	daily	Longitude: -6.020833, 36.3125 Latitude: 30.16667, 46.0000	COB-IEO
7-day increase of sea surface temperature	SST7dinc (ºC)	SST	0.25°	7 days	At sampling sites	COB-IEO
15-day increase of sea surface temperature	SST15dinc (ºC)	SST	0.25°	15 days	At sampling sites	COB-IEO
Weekly average of sea surface chlorophyll-a	CHL_7dL3 (mg m^{-3})	CHL	0.25º	7 days	At sampling sites	COB-IEO

(A)

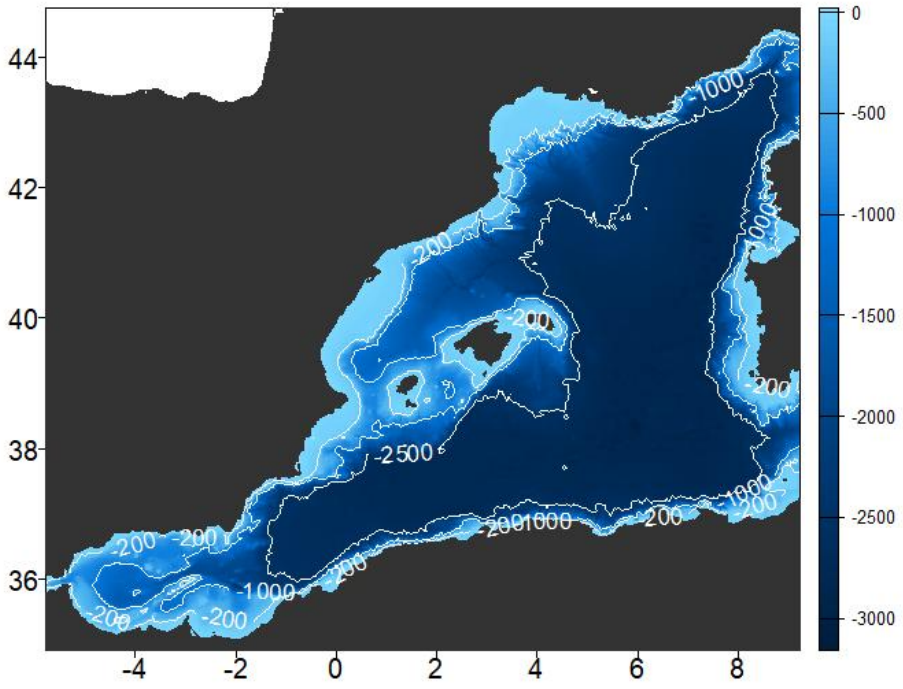

(B)

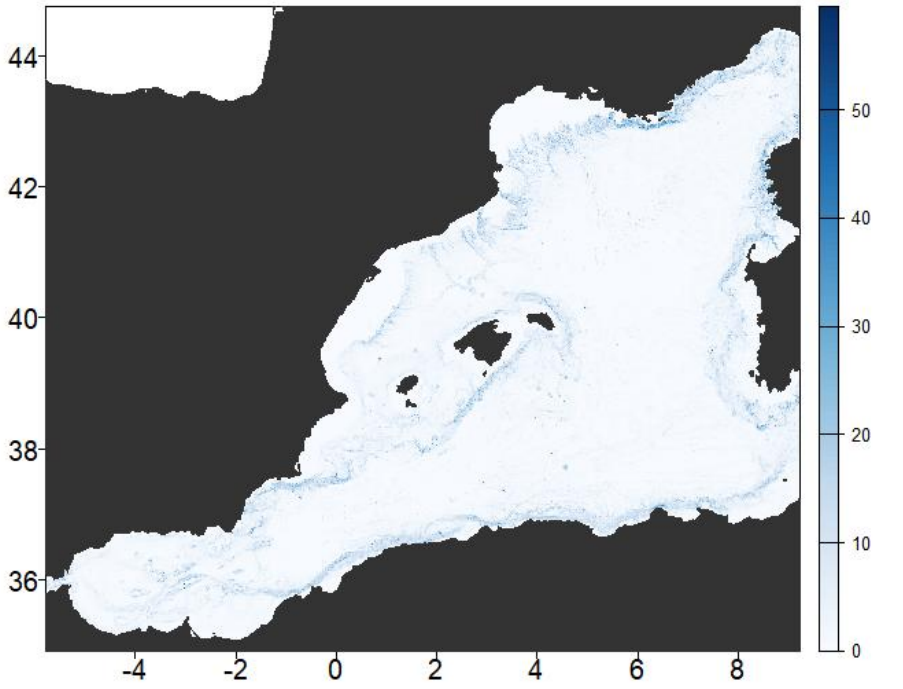

Figure 2.2. Map showing (A) the bathymetry obtained from EMODNET Digital Terrain Model (-200, -1000 and -2500 m are shown) and (B) the derived slope variable (in degrees) for the western Mediterranean.

2.2.5. Area-based environmental analysis

The area-based analysis was designed to characterise the spatial and temporal variability of environmental conditions during the aerial survey sampling window (28 March - 11 July), with the aim of assessing whether variability in features known to influence bluefin tuna (BFT) distribution could affect the observations from the aerial surveys. Analyses were conducted at two spatial scales: (i) a basin scale, encompassing the survey area and adjacent waters to provide regional context, and (ii) the survey polygon defined in Figure 1.

Spatial patterns (2010-2025) in the basin

For each environmental variable, annual mean and standard deviation values were calculated across the full time series (2010-2025). These results were stored in NetCDF files, one per variable, containing both metrics (see Table 2.5). Spatial maps of the mean and standard deviation were generated both annually and over the entire time series, covering the western Mediterranean (Balearic Islands and adjacent waters). These maps were used to characterise the spatial distribution of environmental conditions and their variability (see Results, section 2.3.1). Annual maps were further examined to describe inter-annual variability and the persistence or displacement of spatial features.

Intra- and inter-annual variability within the survey area

Within the survey polygon area (as defined in Figure 2.1), spatially aggregated daily statistics were extracted for each variable. Summary statistics (mean ± standard deviation, SD) were calculated to provide a general reference for environmental conditions during the sampling window. For each variable, boxplots were produced to quantify intra- annual variability within the sampling window and inter-annual variability across years, while line plots were used to examine temporal evolution and the frequency of days exceeding the overall mean (see Results, section 2.3.1).

Together, these analyses provide a comprehensive view of spatial, inter-annual, and intra-annual variability in environmental conditions relevant to standardise BFT observation from the aerial surveys.

2.2.6. Aerial-survey segment-based environmental analysis

Environmental data for the aerial-survey segments environmental data were extracted at a spatial resolution of 0.25° decimal degrees, using a search radius of 0.125° around the mid spatial location (MidLon, MidLat) of the segments. This spatial resolution was chosen as previously having been identified as influencing BFT larval habitat in this same area (Álvarez *et al.,* 2016; Díaz-Barroso *et al.,* 2022). The spatial resolution of the analysis is a very important aspect, as the scale of observation directly affects the capability to identify environmental-ecological relationships (Alvarez-Berastegui *et al.,* 2014). A summary of the variables extracted at each segment mid location is included in Table 2.4.

Table 2.4. Environmental variables for the segments collected from aerial surveys in the Balearic Islands (2010-2025).

Variable	Acronym	Units	Temporal scale	Spatial resolution (decimal degrees)
Bottom depth	Depth	m	-	0.25º
Slope	Slope	degrees	-	0.25º
Sea surface temperature	SST	ºC	daily	0.25º
Sea surface chlorophyll	CHL	mg m^{-3}	daily	0.25º
Sea surface salinity	SSS	-	daily	0.25º
Mixed layer depth	MLD	m	daily	0.25º
Spatial gradient of sea surface temperature	GradSpat_SST	ºC	daily	0.25º
Spatial gradient of sea surface salinity	GradSpat_SSS	-	daily	0.25º
7-day increment of sea surface temperature	sst7dinc	ºC	7 day	0.25º
15-day increment of sea surface temperature	sst15dgrad	ºC	15 day	0.25º

Multivariate analyses of environmental information at segments.

The objective of the multidimensional analysis is to explore a methodology to identify outliers in the environmental data that can have strong influences on the modelling and standardization processes, potentially introducing biases the abundance estimates. Outliers can be attributed either to environmental conditions or to inaccuracies in satellite algorithms or in the physical or biogeochemical models from data sources. These are especially important in areas around river discharges such as the Ebro River. It is important to consider the possibility of excluding the outlier values in the standardization processes.

For the multidimensional analysis all environmental variables measured at the segments centroids were standardised (zero mean, unit variance) prior to multivariate analysis to ensure comparability and to avoid dominance of variables with larger numerical ranges.

A Principal Component Analysis (PCA) was applied to the standardised environmental dataset in order to reduce dimensionality and summarise the main environmental gradients, visualise inter-annual differences in the multivariate environmental space, and identify years characterised by distinct combinations of environmental conditions. The first two principal components (PC1 and PC2) were retained for interpretation and visualisation. Individual observations were projected

onto the PC1–PC2 space and coloured by year. In addition, annual centroids were calculated as the mean PC1 and PC2 scores for each year. In a second step, extremely atypical environmental observations were identified in PCA space as points lying more than three standard deviations from the mean of PC1 or PC2. These points represent rare or extreme environmental combinations.

A sensitivity analysis was conducted by recomputing the PCA after removing these outliers, including re-standardisation of variables and recalculation of annual centroids, to ensure that inter-annual patterns were not driven by a small number of extreme observations.

2.3. Results

2.3.1. Environmental variability within the BFT reproductive area

The results from the area-based analysis examine the short- term variability of the environmental variables within the sampling window (28 March to 11 July) and the inter-annual variability across years (2010-2025) in the study area and its surroundings.

Results show the **basin scale analysis** consisting of: (i) maps of the mean and SD, for each variable, for overall time series (2010-2025), to see a general picture of the oceanographic conditions (Figures 3, 5, 7, 9, 11, 13), and (ii) annual maps of mean and SD survey period, to analyse the inter- annual changes (see Annexes 1.1 - 1.6).

This is followed by the **analysis at the survey area**, consisting of: (i) an overall mean and standard deviation of each variable (2010-2025), and (ii) spatially aggregated summaries in the form of boxplots and line plots, to facilitate the interpretation of temporal variability (Figures 4, 6, 8, 10, 12, 14). In the boxplots, each point represents the daily mean value of the variable within the aerial survey area for each day included in the sampling window.

A summary Table compiling yearly and overall median, mean and SD for each variable was compiled and is presented in Table 2.5.

Table 2.5. Summary statistics of environmental variables in the aerial sampling area between 28 March and 11 July: median, mean and standard deviation (sd) for each year and for the overall analysed period (2010-2025).

	SST			CHL			SSS			MLD			GradSpat_SST			GradSpat_SSS		
Year	**median**	**mean**	**sd**	**median**	**mean**	**sd**	**median**	**mean**	**sd**	**median**	**mean**	**sd**	**median**	**mean**	**sd**	**median**	**mean**	**sd**
2010	21.4	21.7	0.9	0.0655	0.0655	0.0056	37.1	37.0	0.0	12.2	12.7	0.9	1.62	1.64	0.26	0.81	0.86	0.14
2011	22.9	22.5	1.5	0.0627	0.0628	0.0056	36.9	36.9	0.0	11.9	12.1	0.4	1.53	1.57	0.21	1.07	1.07	0.04
2012	22.1	22.4	1.6	0.0625	0.0636	0.0071	37.2	37.2	0.1	11.9	12.0	0.1	1.66	1.68	0.21	0.98	1.00	0.12
2013	20.6	20.5	1.4	0.0689	0.074	0.0164	37.0	37.0	0.1	12.5	13.1	1.3	1.55	1.57	0.33	0.91	1.01	0.21
2014	22.3	22.1	1.5	0.0615	0.0626	0.0059	37.3	37.3	0.1	12.1	12.3	0.5	1.37	1.41	0.18	0.96	0.99	0.12
2015	22.0	22.2	1.7	0.0627	0.0612	0.0063	37.1	37.1	0.0	12.0	12.3	0.7	1.54	1.55	0.20	1.19	1.18	0.10
2016	22.1	22.0	1.0	0.0701	0.0692	0.0084	37.1	37.1	0.0	12.2	12.4	0.5	1.44	1.44	0.16	1.01	0.99	0.07
2017	23.5	22.9	1.5	0.0573	0.0566	0.0038	36.9	36.9	0.0	12.0	12.5	0.8	1.62	1.62	0.18	1.11	1.15	0.14
2018	21.9	21.9	1.6	0.0683	0.0703	0.0113	36.9	36.9	0.1	12.0	12.2	0.4	1.67	1.63	0.28	0.99	0.99	0.13
2019	21.5	21.8	1.7	0.0596	0.0616	0.0098	37.0	37.0	0.0	12.1	12.6	0.8	1.86	1.87	0.22	1.02	1.03	0.06
2020	21.8	22.1	1.5	0.0533	0.0537	0.0048	37.0	37.0	0.1	12.3	12.6	0.9	1.54	1.53	0.22	0.92	0.92	0.09
2021	22.0	22.1	1.6	0.0729	0.076	0.0113	36.8	36.8	0.0	12.0	12.4	1.1	1.52	1.52	0.20	1.06	1.05	0.06
2022	23.7	23.6	1.3	0.0639	0.0659	0.0088	37.2	37.2	0.0	12.0	12.0	0.1	1.71	1.68	0.21	0.95	0.95	0.10
2023	23.1	23.4	1.9	0.0728	0.0742	0.0111	36.9	36.9	0.0	11.9	12.0	0.3	1.34	1.35	0.16	1.15	1.14	0.08
2024	22.5	22.4	1.3	0.0675	0.0681	0.0081	36.8	36.8	0.1	12.5	12.6	0.6	1.48	1.47	0.13	1.47	1.46	0.08
2025	24.8	24.5	2.0	0.0599	0.0618	0.0089	36.8	36.8	0.0	11.9	11.9	0.1	1.49	1.49	0.17	1.26	1.26	0.12
2010-2025	**22.3**	**22.4**	**1.7**	**0.0635**	**0.0654**	**0.0107**	**37.0**	**37.0**	**0.2**	**12.0**	**12.4**	**0.7**	**1.5**	**1.6**	**0.2**	**1.1**	**1.1**	**0.2**

Sea surface temperature (SST)

The mean sea surface temperature (SST) between 28 March to 11 July shows the warmer waters (> 23ºC) concentrated in the vicinity of the Balearic Islands (Figure 2.3). This region also exhibits high variability during the sampling window, with standard deviation values exceeding 1.8ºC (Figure 2.3). Cooler waters (≤ 20ºC) are mainly located near the Strait of Gibraltar and the Gulf of Lion. Inter-annual variability in mean SST during the sampling window is shown in Annex 1.1. Annual SST maps highlight the recurrent location of the 20ºC isotherm in the above-mentioned areas, as well as the persistence presence of warmer waters around the Balearic Islands. The highest mean SST (>24ºC) were observed in 2017, 2022, 2023 and 2025 (Annex 1.1). The year 2025 stands out as exceptionally warm, with almost the entire western Mediterranean basin reaching average SST above 24ºC-25ºC. This is important if SST reaches values, which make adult BFT dive deeper and reduce detectability from the aerial surveys.

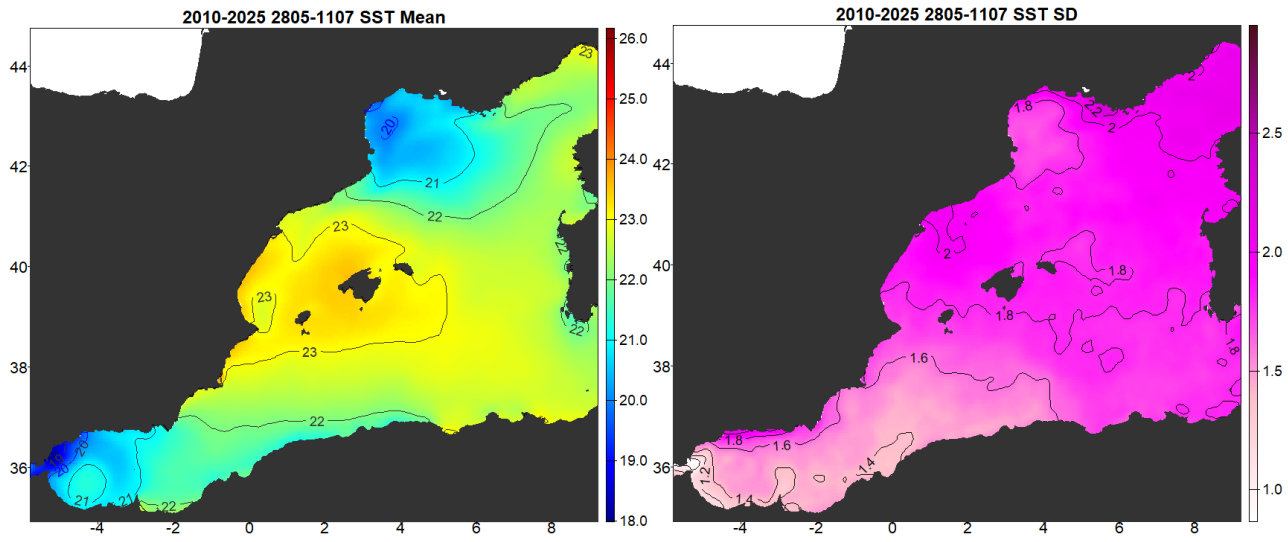

Figure 2.3. Sea surface temperature (SST, ºC): mean (left) and standard deviation (right) between 2010 and 2025 for the survey period (28 March - 11 July).

Mean SST in the study area during the survey window (28 March to 11 July) was 22.4ºC (± 1.7 SD; Table 2.5). Intra-annual variability within this period is relatively similar across years (Figure 2.4). Some years, were noticeably colder, particularly such as 2010 and 2013. In contrast, warmer conditions were observed in 2022 and 2025, with median temperatures of 23.7º and 24.8ºC, respectively (Figure 2.4). Warmer years occur more frequently in the most recent part of the time series (see Figure 2.4). Line plots further indicate an increase over time in the number of days with SST above the overall mean, especially in recent years (Figure 2.4).

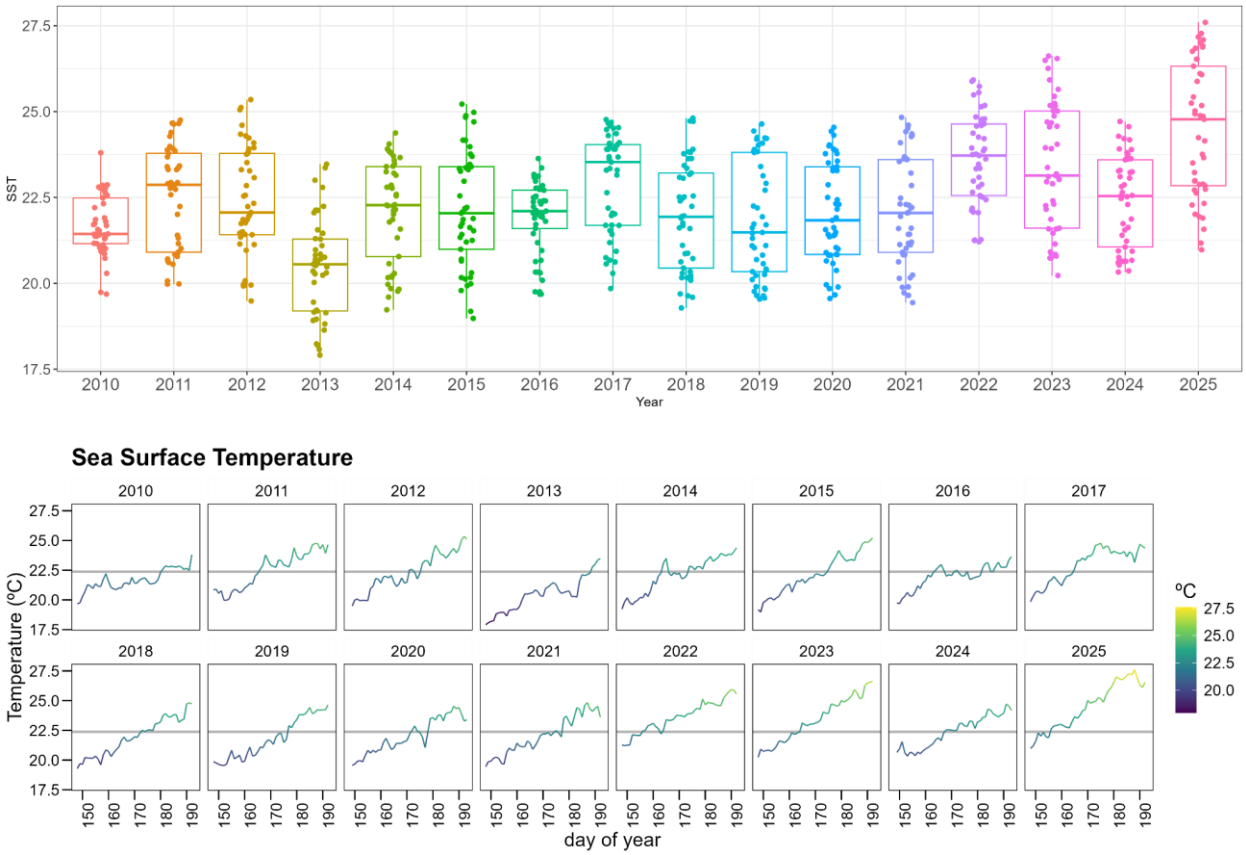

Figure 2.4. Sea surface temperature (SST, ºC): environmental variability in the Balearic Island BFT spawning area for the period 2010-2025. The upper panel shows annual boxplots and lower panel line plots. In the line plots, the grey horizontal line indicates mean for the whole period.

Chlorophyll-a (CHL)

The spatial distribution of mean chlorophyll-a (CHL) between 28 March to 11 July indicates the presence of low-productivity waters between the Balearic Islands, Corsica and Sardinia. This oligotrophic area extends southwards towards the North African coast (Figure 2.5). This region is delineated by the -1.2 CHL isoline in natural logarithmic scale, corresponding to 0.82 mg m-3. Higher productivity waters are observed in the Gulf of Lion, the western Alboran Sea, and the Ebro Delta. These areas also exhibit the highest variability, with standard deviation values exceeding -1.4 in log-scale CHL (equivalent to 0.2 mg m-3) (Figure 2.5). Annual maps of mean CHL (Annex 1.2) reveal marked interannual variability in the position of the -1.2 log-scale CHL isoline. This variability reflects year-to-year changes in the spatial extent of the most oligotrophic waters. In 2017, the low-productive area ws considerably more extensive than the mean pattern (Figure 2.5). In contrast, in 2018 it was markedly reduced and largely confined to areas south of the Balearic Islands.

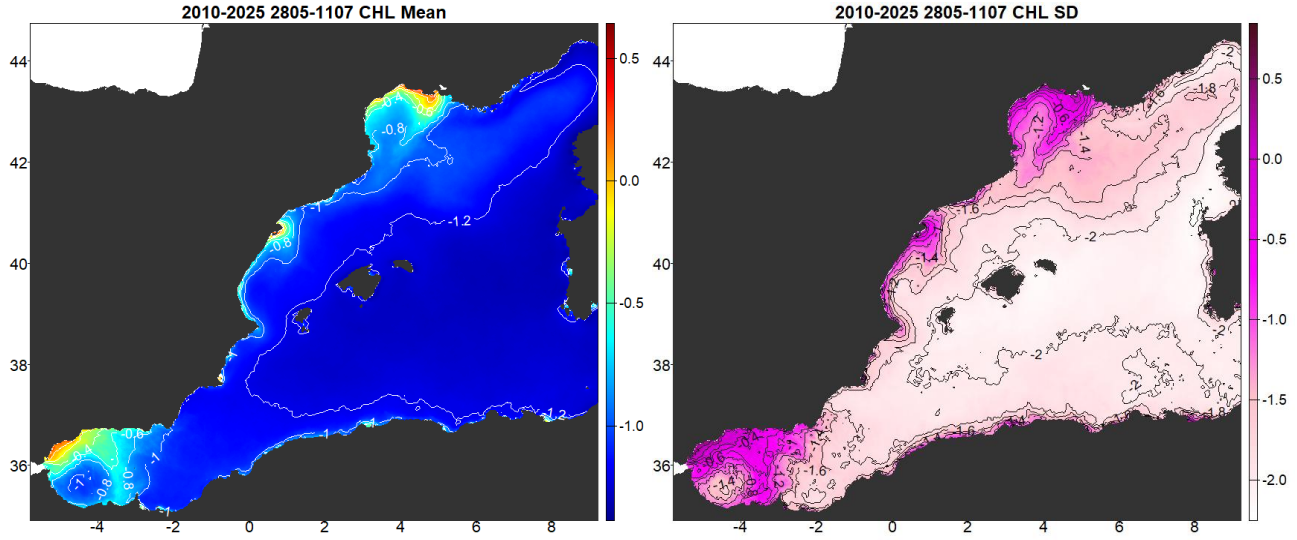

Figure 2.5. Sea surface chlorophyll-a (CHL, log10 (mg m^{-3}): mean (left) and standard deviation (right) between 2010 and 2025 for the survey period (28 March - 11 July).

Mean chlorophyll-a in the study area is low, with average concentration of 0.0654 mg m^{-3} (± 0.0107 SD; Table 2.5). Boxplots indicate that intra-annual variability between 28 March and 11 of July is greater than the variability between years (Figure 2.6). Some years, such as 2017 and 2020, show consistently low CHL values, whereas others, notably 2013, display a wider intra-annual variability and median values (Figure 2.6). Line plots reveal episodic sharp increases in daily CHL concentrations in the area in some specific years, such as around day 180 in 2013, day 170 in 2021, and a more temporally limited increase around day 160 in 2018 (Figure 2.6).

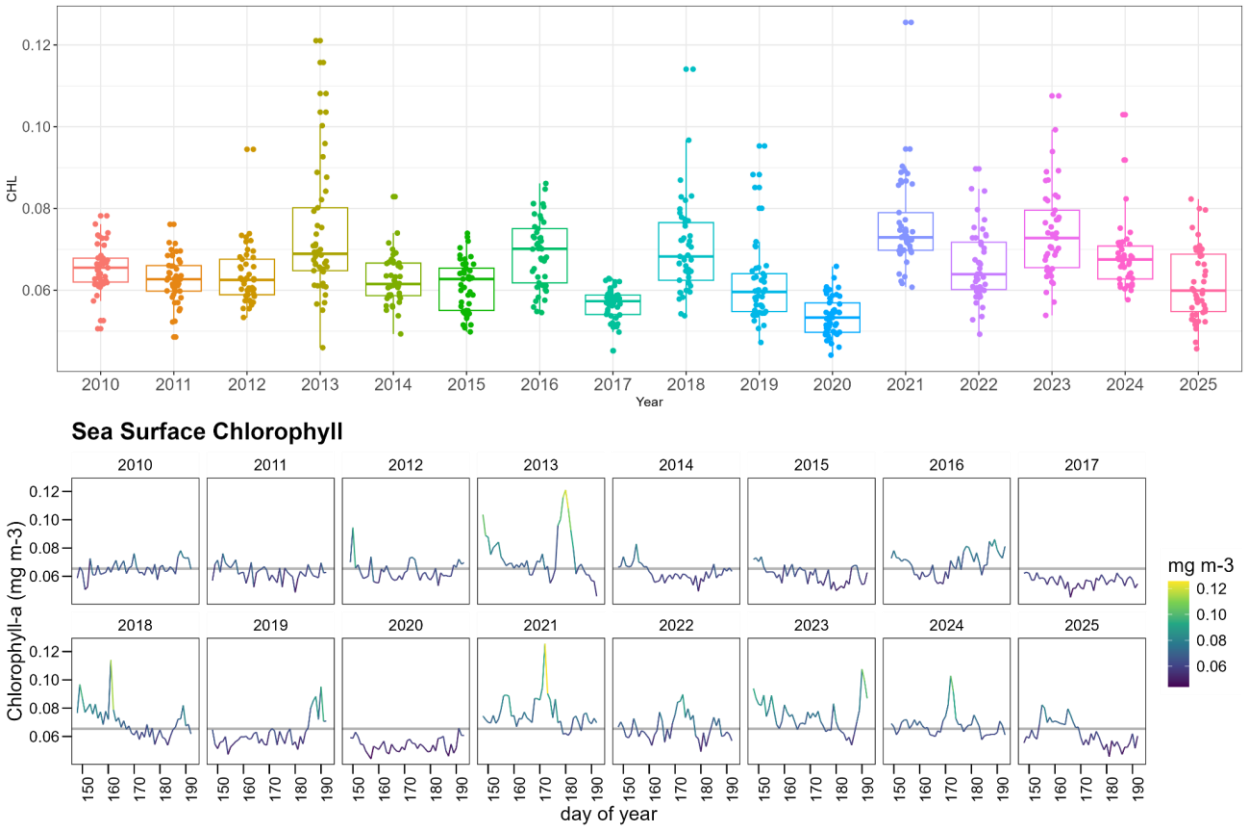

Figure 2.6. Sea surface chlorophyll-a (CHL, mg/m^3): environmental variability in the Balearic Island BFT spawning area for the period 2010-2025. The upper panel shows annual boxplots and lower panel line plots. In the line plots, the grey horizontal line indicates mean for the whole period.

Sea surface salinity (SSS)

The map of mean sea surface salinity (SSS) during the sampling window (28 March - 11 July) for the period 2010-2025 shows lower salinity values (< 37.5) south of the Balearic Islands and in limited areas influenced by major river outflows, i.e. the Po and the Ebro rivers (Figure 2.7). Values below 35.0 were excluded for visualisation purposes and are shown as white grid cells. Spatial variability in SSS is higher in regions with elevated salinity values, whereas the lowest standard deviation is observed in open-ocean waters far from the coast (Figure 2.7). Annual maps of mean SSS for the period 28 March-11 July (Annex 1.3) highlight inter-annual shifts in the position of the 37.5 isohaline. Depending on the year, this feature is located within the Balearic channels (e.g. 2019, 2020, 2023, 2024), displaced northwards (e.g. 2011, 2017), or shifted southwards (e.g. 2012, 2013).

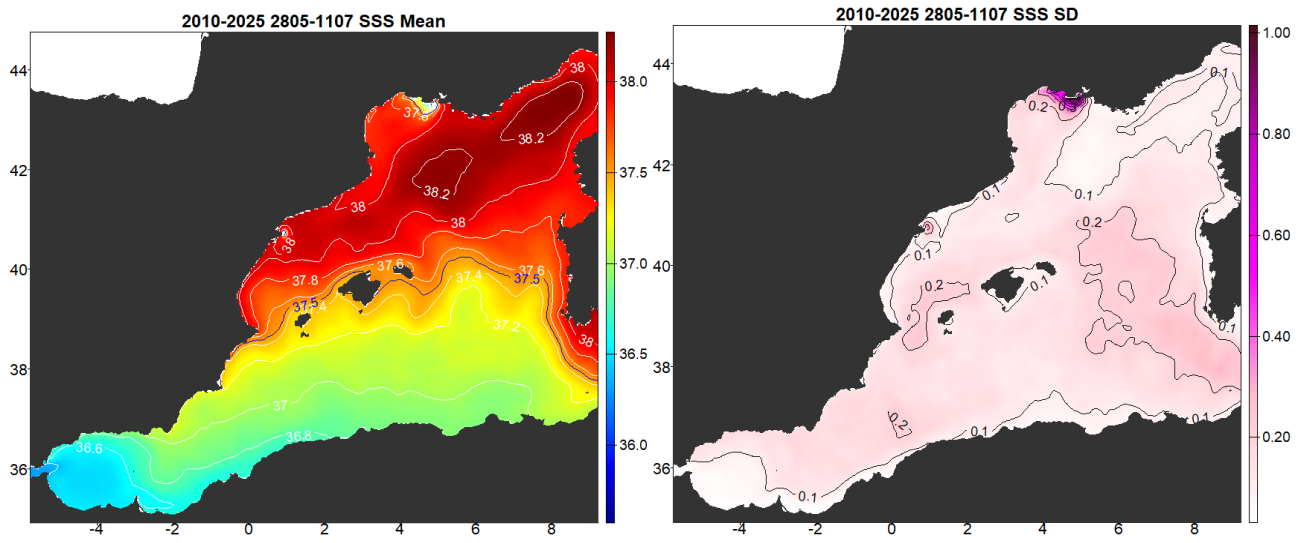

Figure 2.7. Sea surface salinity (SSS, psu): mean (left) and standard deviation (right) between 2010 and 2025 for the survey period (28 March - 11 July).

Mean SSS in the study area during the sampling period was 37.0 (±0.2 SD; Table 2.5). Inter-annual variability in SSS is greater than intra-annual variability (Figure 2.8), generally varying by less than one salinity unit (ranging from 36.7 to 37.4). Years such as 2012, 2014-2016 and 2022 show consistently higher-than-average SSS, whereas 2011, 2017, 2021, and 2023-2025 are characterised by values below the overall mean. Joint interpretation of these boxplots and annual maps in Annex 1.3, suggests that years with higher mean SSS coincide with a southward displacement of the 37.5 isopycnal, indicating a wider spatial extent of the more saline Mediterranean waters and a reduced influence of recently advected Atlantic waters.

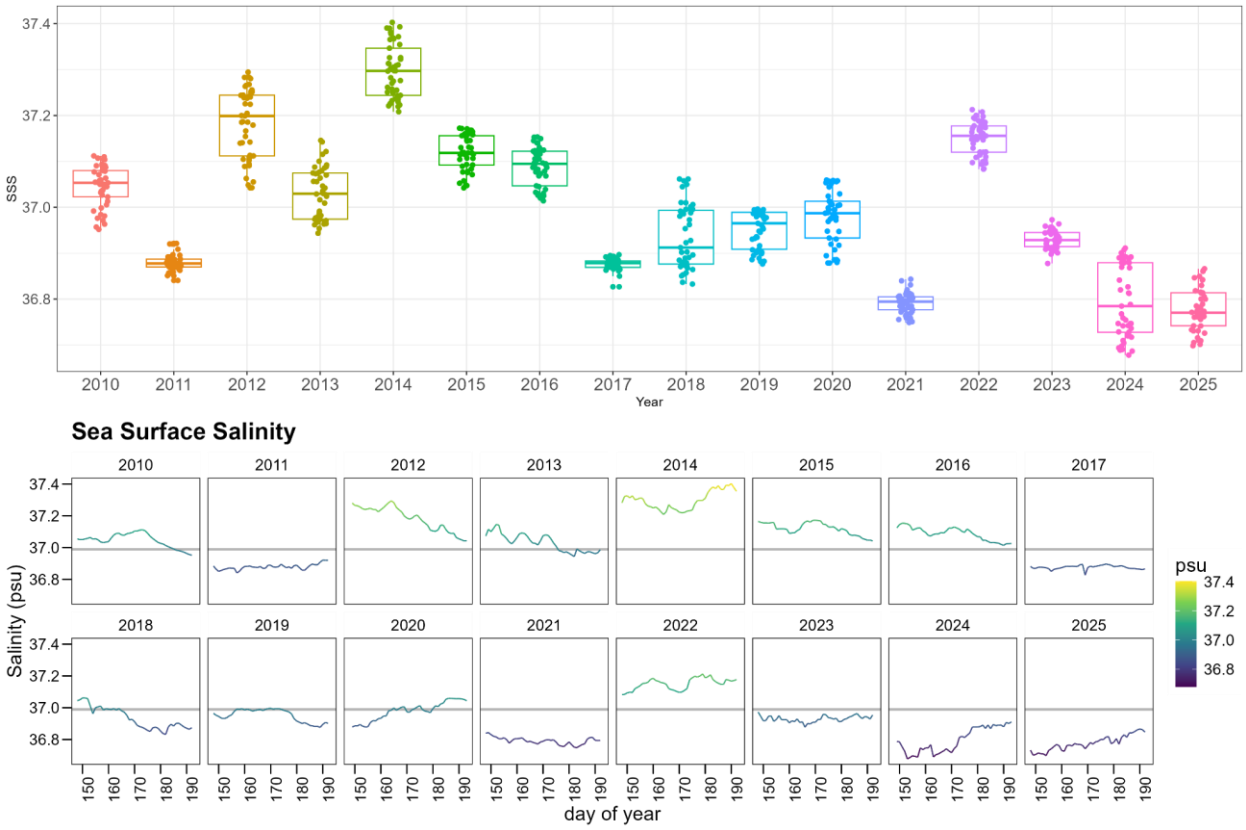

Figure 2.8. Sea surface salinity (SSS, psu): environmental variability in the Balearic Island BFT spawning area for the period 2010-2025. The upper panel shows annual boxplots and lower panel line plots. In the line plots, the grey horizontal line indicates mean for the whole period.

Depth of the mixed layer (MLD)

During the sampling window (28 March–11 July), mixed layer depth (MLD) is shallowest and least variable in the area between the Balearic Islands and the mainland (Figure 2.9). In this region, mean MLD values are approximately 12 m, with low variability (<0.5 m SD). Slightly deeper mixed layers are observed south of the Balearic Islands, with mean values around 13 m (Figure 2.9). Annual maps of mean MLD (Annex 1.4) show interannual variability in the spatial distribution of MLD across the study area. However, MLD values around the Balearic Islands remain relatively stable from year to year.

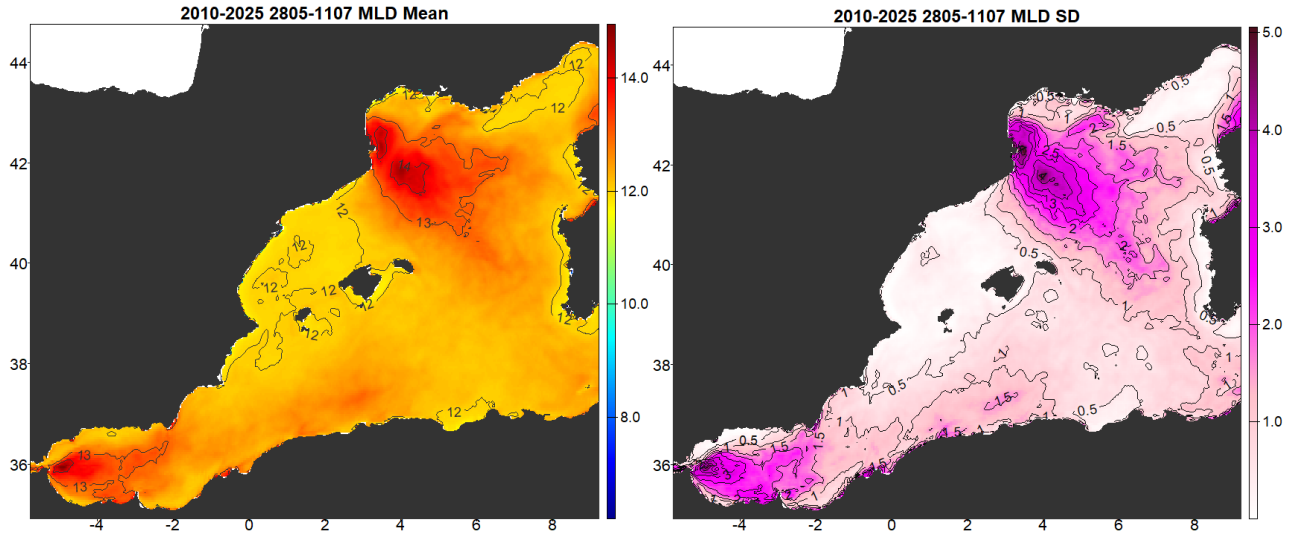

Figure 2.9. Depth of the mixed layer (MLD, m): mean (left) and standard deviation (right) between 2010 and 2025 for the survey period (28 March - 11 July).

The mean MLD in the study area was around 12.4 m (± 0.7 SD, Table 2.5). In most years, intra-annual variability in MLD is not great, with some years showing extremely low variability. This is the case in 2012, 2022 and 2025 when all daily values showed little fluctuation, remaining very close to 12 m (Figure 2.10). Such stability suggests that, within these years, changes in MLD are unlikely to introduce substantial variability in species observations attributable to environmental conditions. In contrast, years with greater intra-annual variability in MLD may present different environmental contexts for the species, potentially affecting their distribution or detectability. However, MLD is a model outcome and validation exercises should be performed.

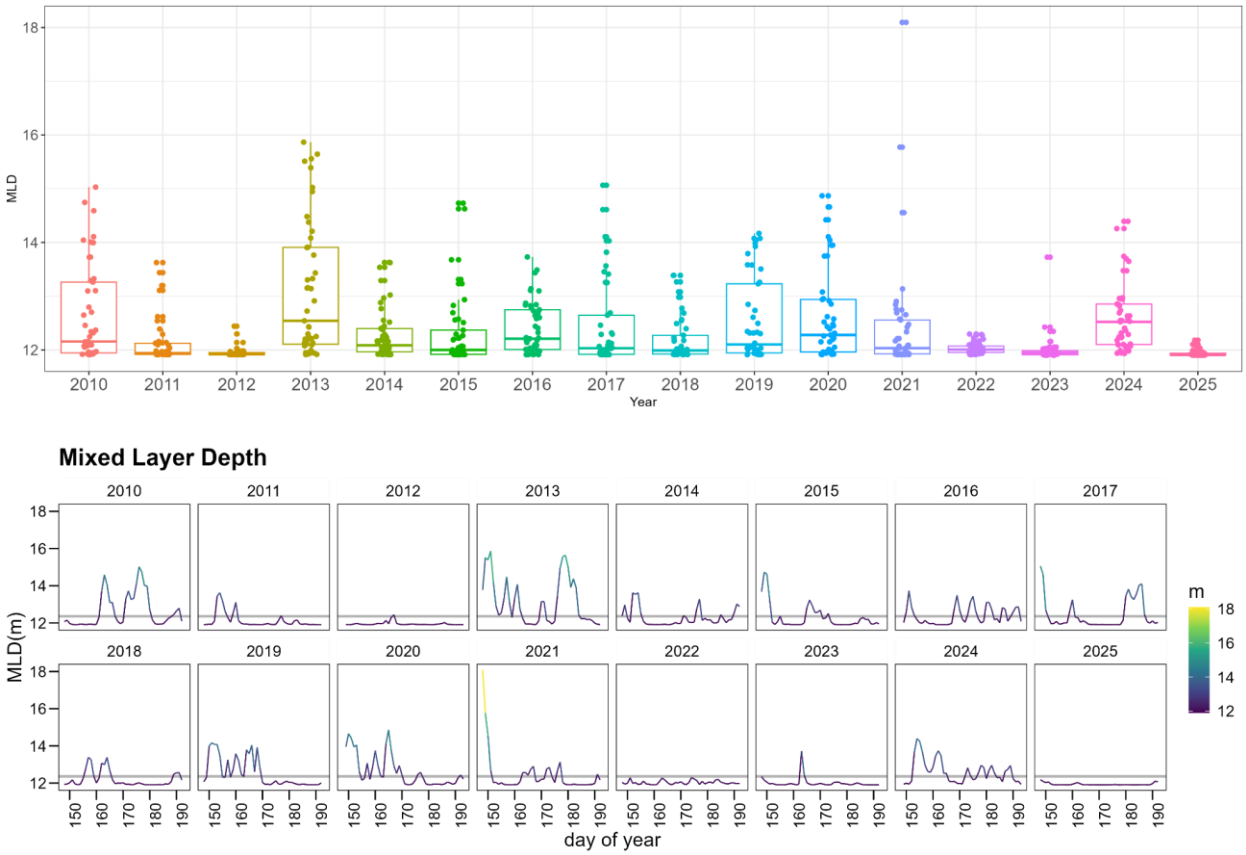

Figure 2.10. Depth of the mixed layer (MLD, m): environmental variability in the Balearic Island BFT spawning area for the period 2010-2025. The upper panel shows annual boxplots and lower panel line plots. In the line plots, the grey horizontal line indicates mean for the whole period.

Spatial gradient of sea surface temperature (GradSpat_SST)

The spatial gradient of sea surface temperature (SST) in the vicinity of the Balearic Islands shows relatively low mean values, around 2 °C (±1 °C SD), compared with other areas of the western Mediterranean (Figure 2.11). Higher mean spatial gradients and greater variability are observed near the Strait of Gibraltar, associated with the inflow of Atlantic waters. Elevated gradients are also evident in regions potentially influenced by coastal upwelling, particularly in the Gulf of Lion and, to a lesser extent, along the Algerian coast and the western coast of Corsica. Annual maps of mean SST spatial gradients during the survey window (28 March–11 July) (Annex 1.5) show patterns broadly consistent with the long-term mean presented in Figure 2.11. Inter-annual differences are mainly reflected in changes in the intensity of potential coastal upwelling. Reduced gradients are observed in the Gulf of Lion in some years (e.g. 2012, 2014, 2020), whereas intensified gradients occur along the northern Algerian coast in others (e.g. 2017, 2025).

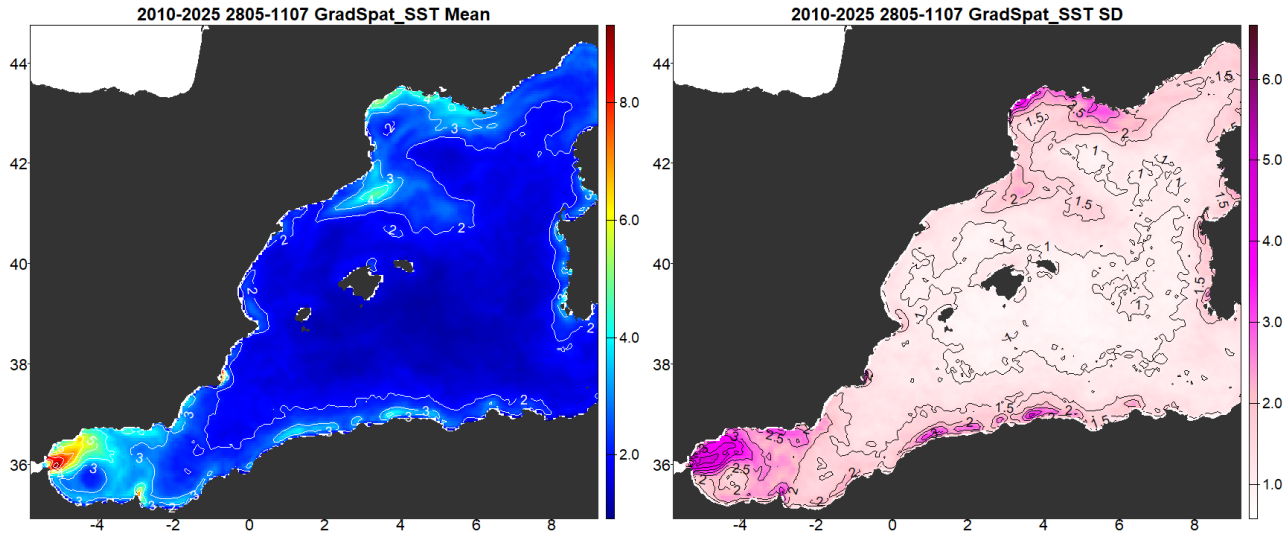

Figure 2.11. Spatial gradient of SST (GradSpat_SST, ºC): mean (left) and standard deviation (right) between 2010 and 2025 for the survey period (28 March - 11 July).

The mean spatial gradient of SST (GradSpat SST) in the study area was 1.6 (± 0.2 SD, Table 2.5). Boxplots show that GradSpat SST do not vary greatly between years and, in general, the amount of intra-annual variability is similar among the years (Figure 2.12). However, 2013 and 2018 showed a wider range of daily GradSpat SST, whereas 2016 and 2024 and 2025 showed lower intra-annual variability. Line plots further show that the daily Grad Spat SST values generally fluctuate around the average GradSpat SST, and only rarely show intra-annual temporal trends (Figure 2.12).

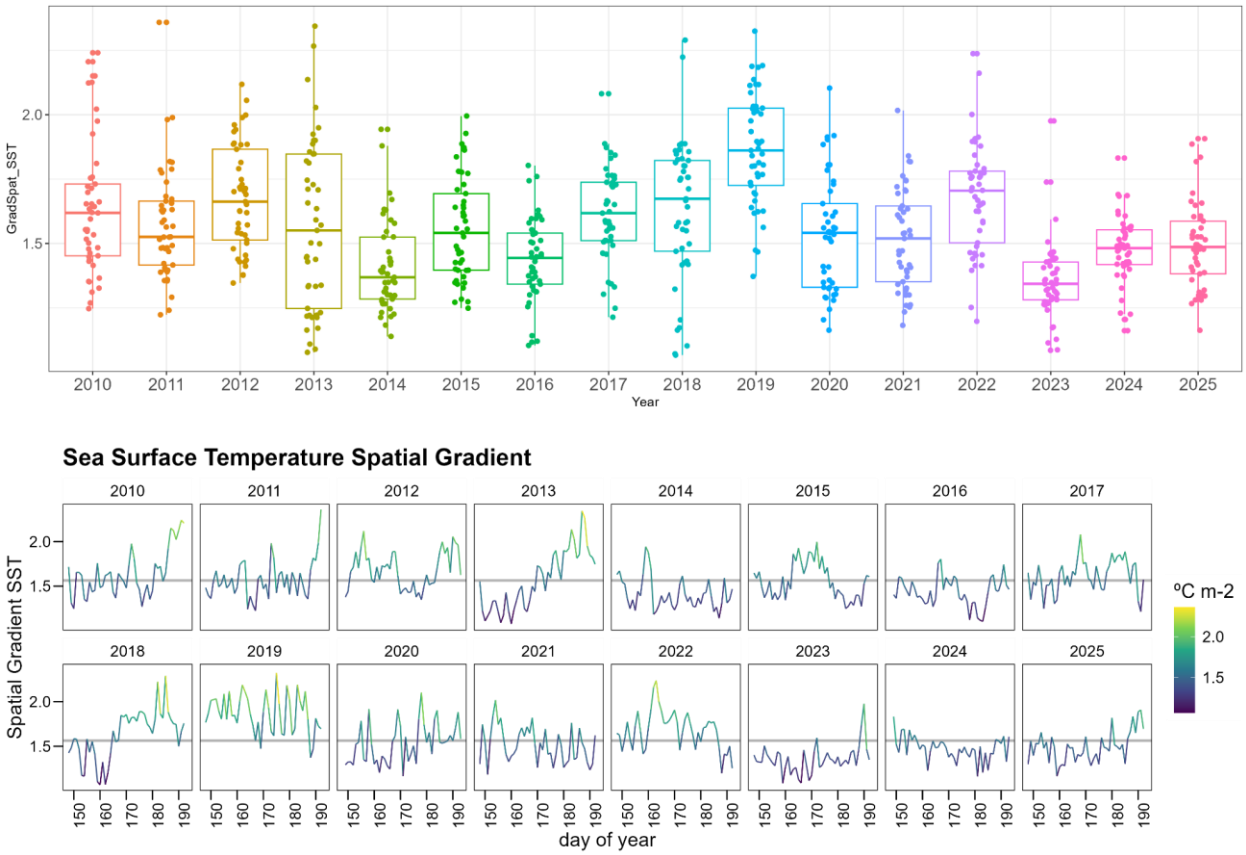

Figure 2.12. Spatial gradient of SST (GradSpat_SST, ºC): environmental variability in the Balearic Island BFT spawning area for the period 2010-2025. The upper panel shows annual boxplots and lower panel line plots. In the line plots, the grey horizontal line indicates mean for the whole period.

Spatial gradient of sea surface salinity (GradSpat_SSS)

The highest spatial gradients of sea surface salinity (GradSpat SSS) occur near major river mouths (Figure 2.13). These areas also show the highest standard deviation values, indicating elevated variability. In the vicinity of the Balearic Islands, the strongest salinity gradients are observed along the northern coasts. These gradients coincide with areas of increased variability (Figure 2.13). Annual maps of GradSpat SSS reveal marked inter-annual variability in their spatial distribution (Annex 1.6). In recent years (2023–2025), an intensification of salinity spatial gradients is evident around the Balearic Islands.

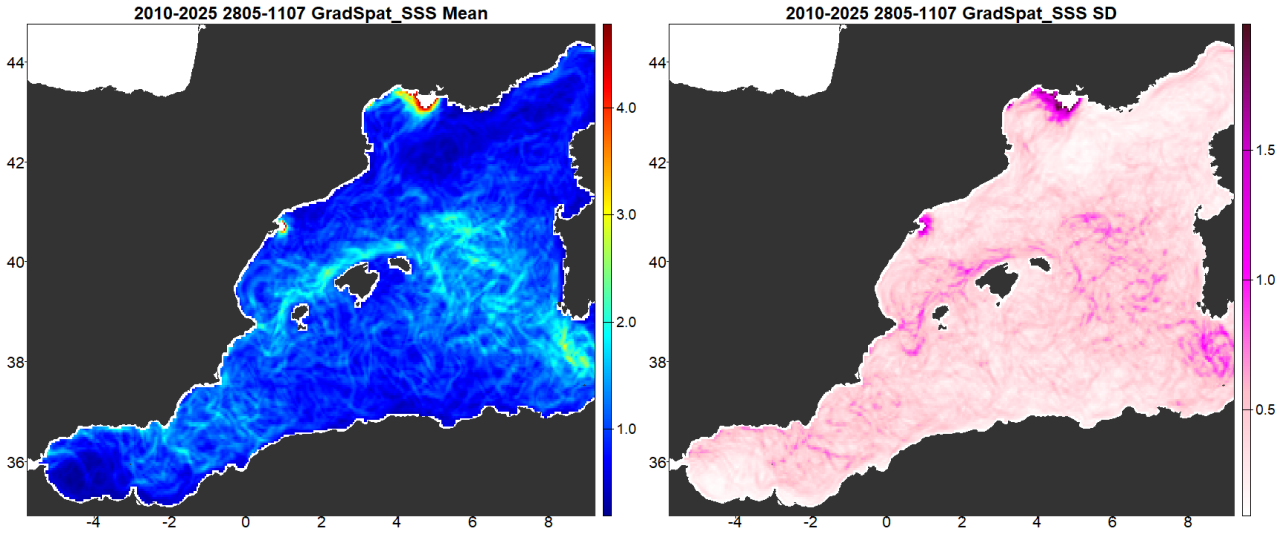

Figure 2.13. Spatial gradient of SSS (GradSpat_SSS, psu): mean (left) and standard deviation (right) between 2010 and 2025 for the survey period (28 March - 11 July). Note that mean values above 5.0 and SD values above 2.0, always located in the river mouths, were filtered for visualisation purposes and appear white grid cells in the maps.

The mean GradSpat SSS was 1.0 (± 0.2 SD, Table 2.5). The inter-annual variability is generally greater than the intra-annual variability, except for 2013, which shows high variability within the sampling window (Figure 2.14). Most values in 2011, 2015, 2017, and in 2023-2025 are above the overall mean, with the highest values observed in 2024. Line plots show no consistent temporal pattern within the sampling window (Figure 2.14), with some years showing relatively stable values and others exhibiting increasing or decreasing tendencies (Figure 2.14).

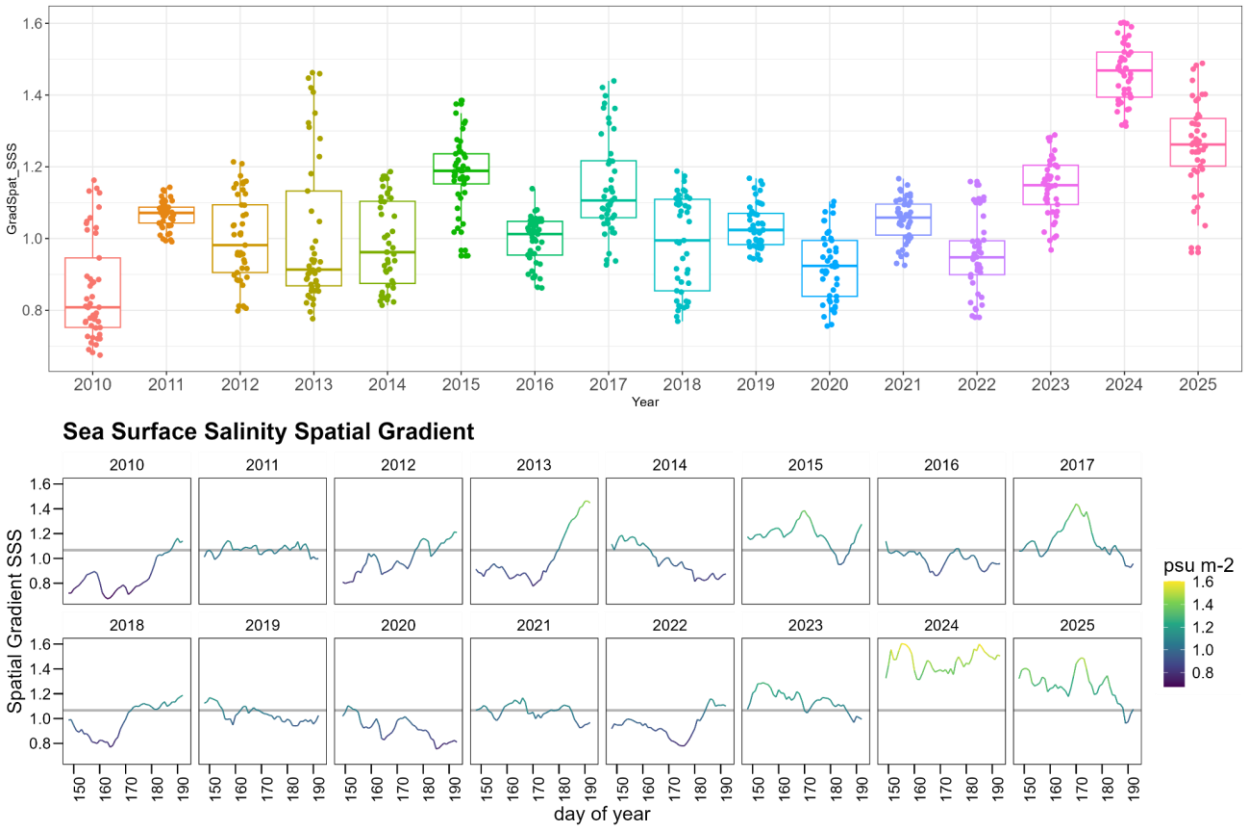

Figure 2.14. Spatial gradient of sea surface salinity (GradSpat_SSS, psu): environmental variability in the Balearic Island BFT spawning area for the period 2010-2025. The upper panel shows annual boxplots and lower panel line plots. In the line plots, the grey horizontal line indicates mean for the whole period.

Day of the year when SST threshold is reached

The day of the year at which mean SST in the survey area polygon exceeded the 20ºC (commonly recognised as BFT start of the spawning) was analysed. It shows a statistically significant advancement, at a rate of 0.49 days per year (Figure 2.15A). The day at which the higher temperatures (>24ºC) were reached also increased and at a higher rate of 1.94 days per year.

(A)

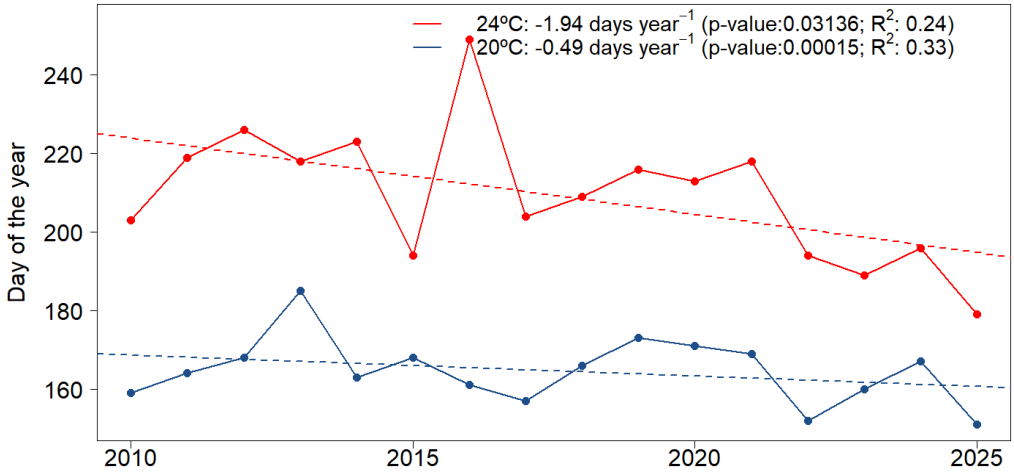

(B)

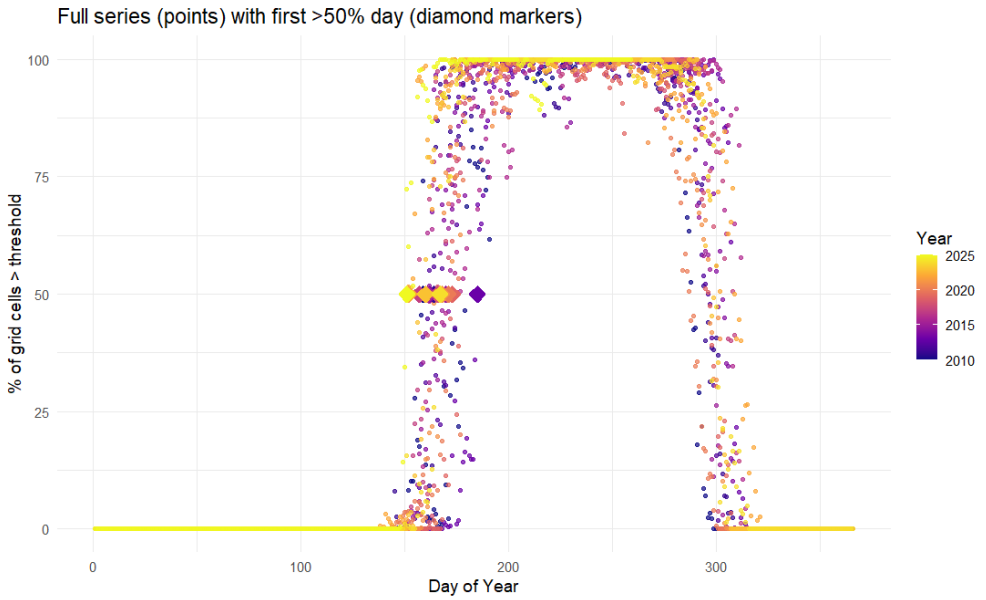

Figure 2.15. Seasonal progression of sea surface temperature (SST): **(A)** day of the year at which average temperature is above the selected 20ºC (24ºC threshold also shown) and (**B**) percentage of cells in the area that are above the 20ºC threshold for each day year and year. Diamonds indicate the day of the year at which 50% of the cells in the area are above 20ºC.

Current intensity in the Ibiza Channel

Mean surface current velocity in the Ibiza Channel was 0.2 m s^{-1}. Time series of absolute surface current velocity show significant inter-annual differences (Figure 2.16). Some years exhibit a wide range of velocities, particularly 2014. In contrast, other years show lower within-year variability, including 2015, 2016, 2021, 2022, and 2024. A key result of this analysis is the presence of significant inter-annual differences in surface currents within the area covered by the radar system. These differences indicate that, during the period of adult arrival, distinct environmental conditions prevailed in the Ibiza Channel. This area plays a critical role in regulating the intrusion of Atlantic waters and may influence whether adult BFT are distributed towards the southern part of the archipelago or towards northern areas.

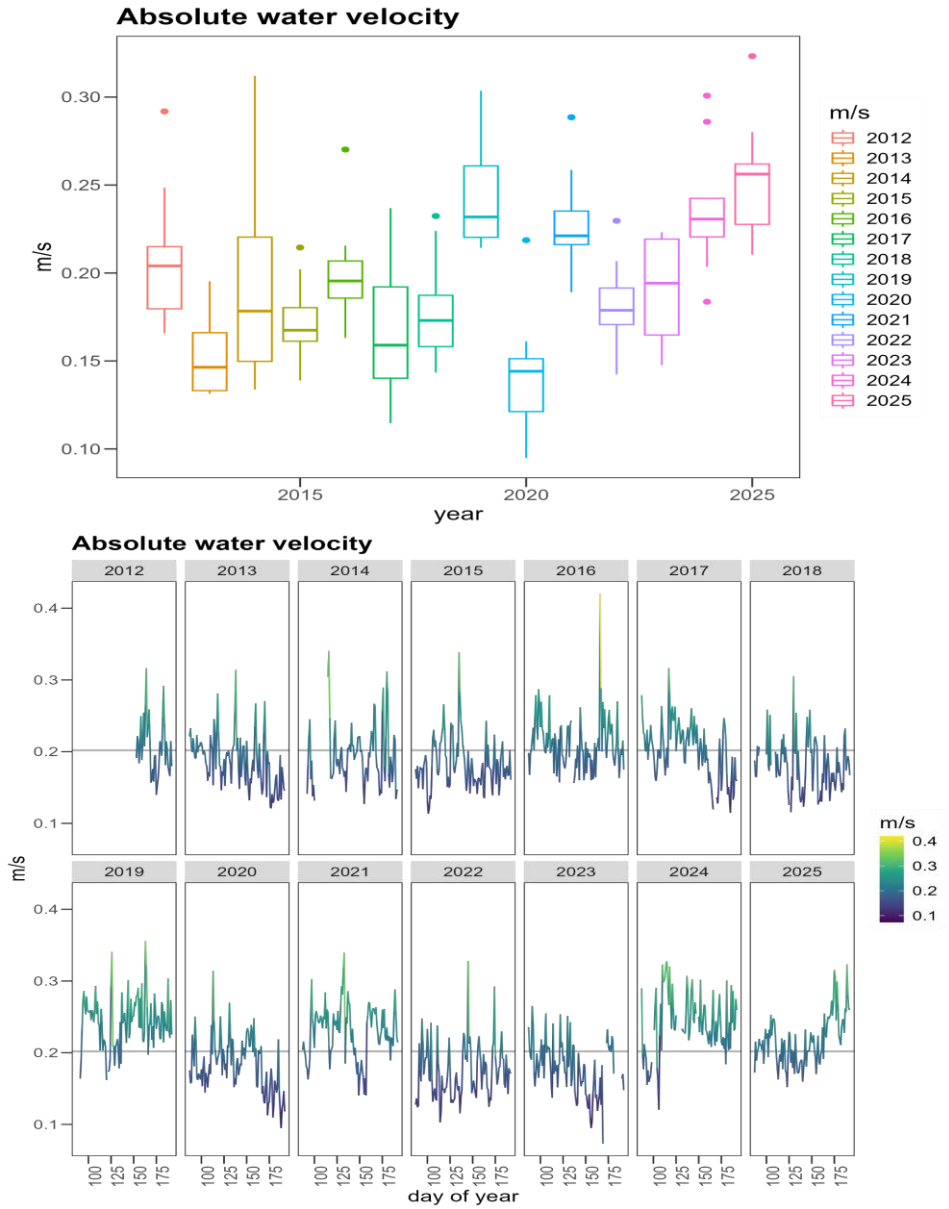

Figure 2.16. Current velocity at the Ibiza Channel (m s^{-1}) for the aerial survey period (25 March - 11 July). Note that there was no available data for the years 2010-2011, and also for the first days of the sampling window in 2012.

2.3.2. Environmental variability within aerial survey segments

The analysis of the environmental variability at the aerial survey segments is shown in the form of boxplots showing the intra-annual variability. Dots represent the variability within each survey. A summary statistics Table 2.is also presented (Table 2.6).

Bathymetry (Depth)

The mean bottom depth in the segment's MidLon-MidLat location was 1228 m (± 776 m SD; Table 2.6). Intra-annual variability is generally bigger than inter-annual variability (Figure 2.17). Recent years (2022-2025) sampling seem to be slightly more concentrated at deeper waters, with median values around -1,500 m while in the earlier years (2010-2017) median bottom depth was around -1,000 m (Figure 2.17).

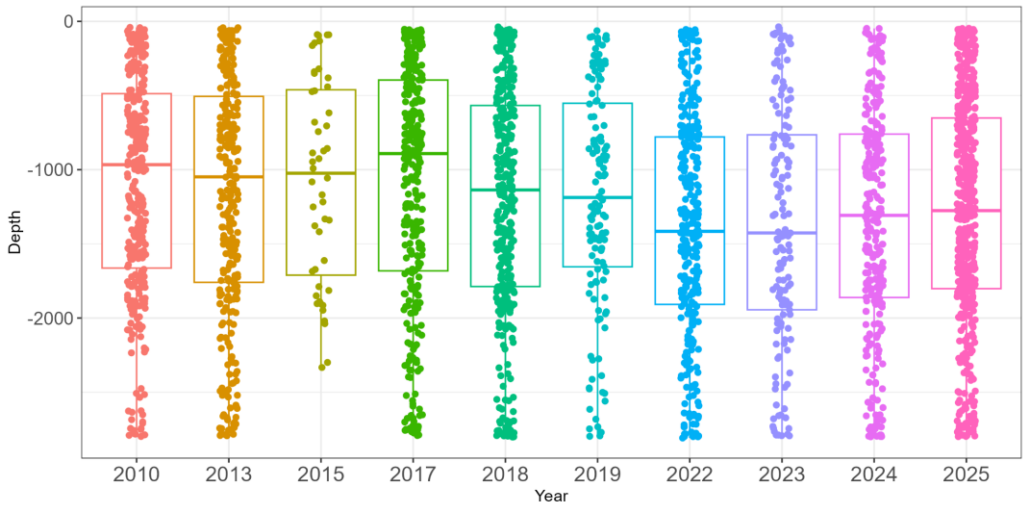

Figure 2.17. Bathymetry (Depth, m): environmental variability in the aerial survey sampling segments for the period 2010-2025.

Slope (Slope)

The mean slope in the segment's MidLon-MidLat location was 2.3 degrees (± 1.6 SD; Table 2.6). Similar to bathymetry, intra-annual variability is generally bigger than inter-annual variability (Figure 2.18), but no differences are seen in the distribution of slope values in the recent years compared to the earlier years. The year 2015 seems to be the most different that could be attributed to a smaller coverage.

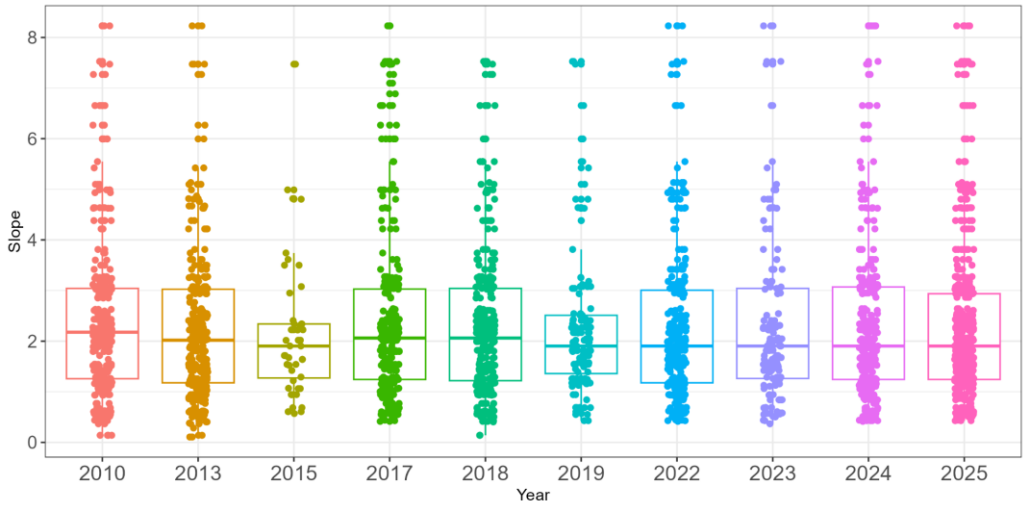

Figure 2.18. Slope (Slope, degrees): environmental variability in the aerial survey sampling segments for the period 2010-2025.

Sea surface temperature (SST)

The mean sea surface temperature (SST) in the segment's MidLon-MidLat location was 23.3 ºC (± 1.8 Mean sea surface temperature (SST) at the segment mid-point locations (MidLon–MidLat) was 23.3 °C (±1.8 SD; Table 2.6). Significant interannual differences in SST are observed and may influence aerial survey detections (Figure 2.19). In most years, SST values along survey segments exceed 20 °C, the thermal threshold associated with the onset of Atlantic bluefin tuna spawning. An exception occurs in 2019, when SST was significantly lower. In this year, reduced temperatures may have negatively affected BFT observations if adult aggregations had not fully developed at the time of the surveys. High SST values are observed in 2015, 2022, and 2025, with median temperatures close to or exceeding 25.0 °C. In 2015, elevated SST values are partly attributable to sampling concentrated in warmer areas. In contrast, in 2022 and 2025, high SST reflects generally warm conditions across the study area. Such elevated temperatures may also have negative effects on BFT detectability during aerial surveys.

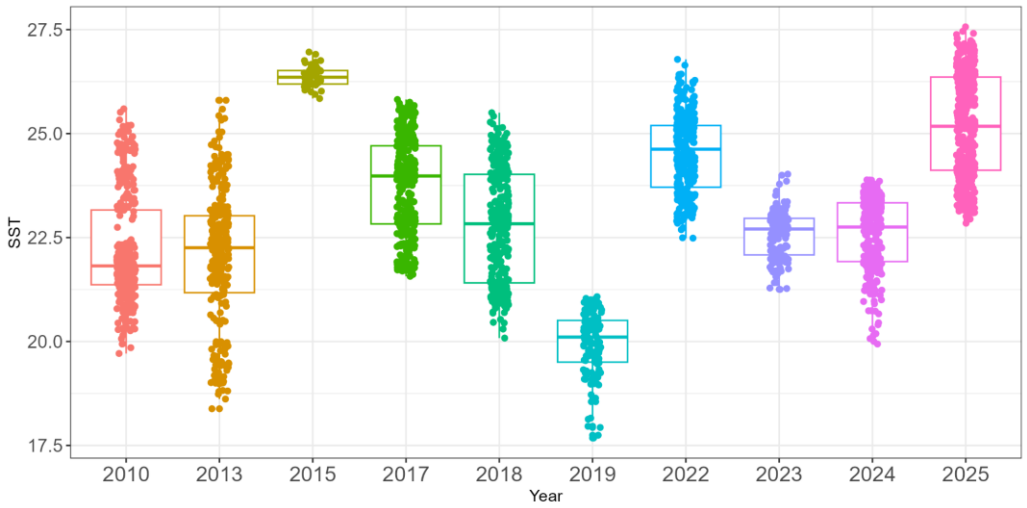

Figure 2.19. Sea surface temperature (SST, ºC): environmental variability in the aerial survey sampling segments for the period 2010-2025.

Sea surface chlorophyll-a (CHL)

The mean sea surface chlorophyll-a (CHL) in the segment's MidLon-MidLat location was 0.0658 mg m^{-3} (± 0.0486 SD; Table 2.6). Daily CHL values are low and seem pretty stable throughout the period, with some years showing higher surface productivity like 2010, 2013, 2015 and 2024 (Figure 2.20). There are very few locations at which CHL concentration was really high (> 0.25 mg m^{-3}). This is the case for three spots in the year 2013 and one spot in 2018, not seen in the other years. These values should be further inspected and the convenience of their inclusion in future modelling steps be discussed.

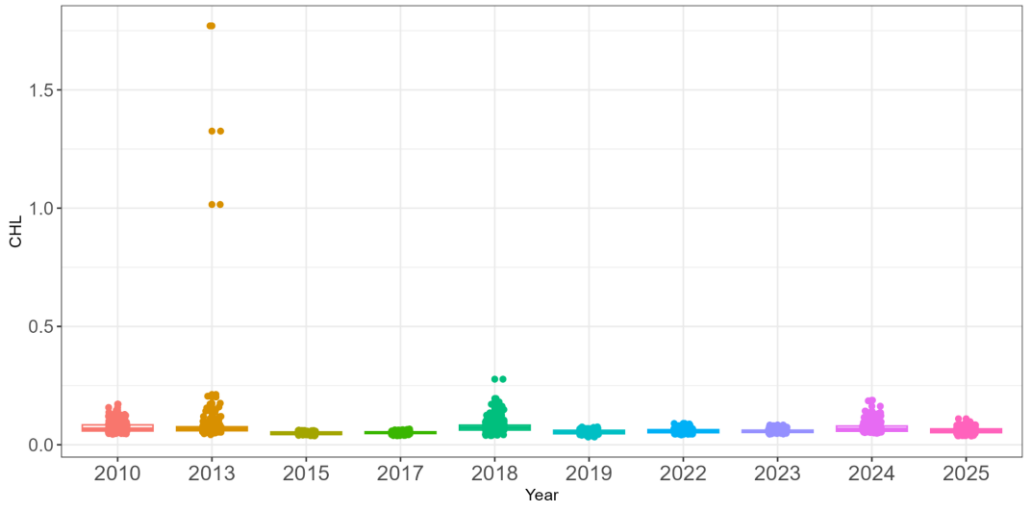

Figure 2.20. Sea surface chlorophyll-a (CHL, mg m^{-3}): environmental variability in the aerial survey sampling segments for the period 2010-2025.

Sea surface salinity (SSS)

The mean sea surface salinity (SSS) in the segment's MidLon-MidLat location was 37.4 (± 0.4 SD; Table 2.6). The SSS in the sampling area seem to show a descending trend in the median values observed in the segment's locations (Figure 2.21). This can be indicative of increased influence of recently advected Atlantic waters, which are less saline. This effect can have relevant implications on the spatial distribution of adults within the sampling area.

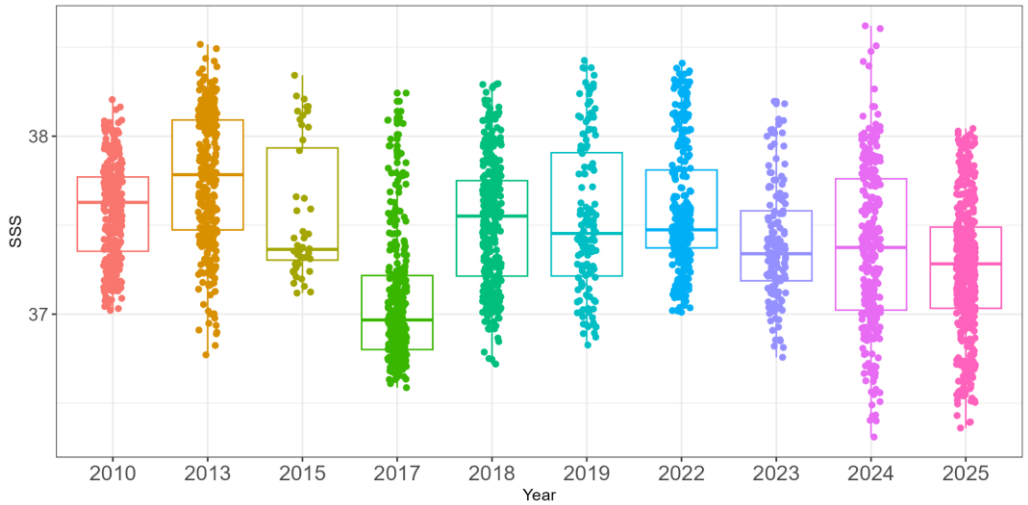

Figure 2.21. Sea surface salinity (SSS, psu): environmental variability in the aerial survey sampling segments for the period 2010-2025.

Depth of the mixed layer (MLD)

The mean depth of the mixed layer in the segment's MidLon-MidLat locations was 12.0 m (± 0.5 SD; Table 2.6). Values remain pretty stable throughout the time series (Figure 2.22), with significant differences at certain locations with high mean values (> 14 m), like in years 2010, 2013, 2017, 2019, 2023 and 2024.

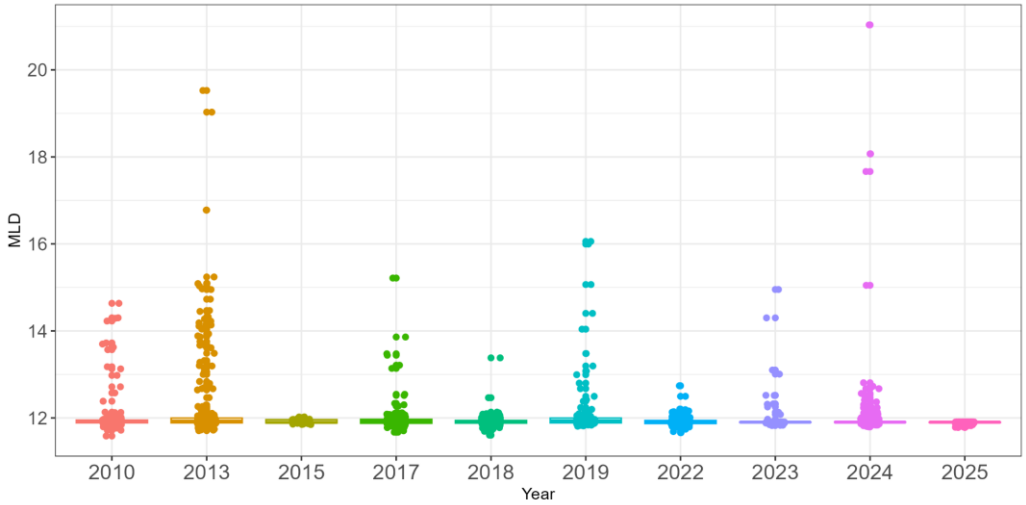

Figure 2.22. Depth of the mixed layer (MLD, m): environmental variability in the aerial survey sampling segments for the period 2010-2025.

Table 2.6. Summary statistics of environmental variables in the aerial survey segments between 28 March and 11 July: median, mean and standard deviation (sd) for each year and for all surveys compiled together (2010-2025).

	Bathy			Slope			SST			CHL			SSS		
Year	**median**	**mean**	**sd**	**median**	**mean**	**sd**	**median**	**mean**	**sd**	**median**	**mean**	**sd**	**median**	**mean**	**sd**
2010	-966	-1090	735	2.2	2.5	1.7	21.8	22.2	1.3	0.0671	0.0741	0.0225	37.6	37.6	0.3
2013	-1048	-1170	806	2.0	2.3	1.5	22.3	22.1	1.6	0.0661	0.0852	0.1349	37.8	37.8	0.4
2015	-1024	-1078	684	1.9	2.1	1.3	26.4	26.4	0.2	0.0463	0.0482	0.0072	37.4	37.6	0.4
2017	-892	-1100	806	2.1	2.4	1.7	24.0	23.7	1.2	0.0515	0.0512	0.0053	37.0	37.1	0.4
2018	-1137	-1213	771	2.1	2.3	1.5	22.8	22.8	1.3	0.0723	0.0761	0.0244	37.6	37.5	0.4
2019	-1187	-1191	749	1.9	2.3	1.4	20.1	20.0	0.8	0.0526	0.0539	0.0092	37.5	37.5	0.4
2022	-1416	-1387	762	1.9	2.3	1.6	24.6	24.5	0.9	0.0576	0.0583	0.0091	37.5	37.6	0.4
2023	-1426	-1365	800	1.9	2.4	1.7	22.7	22.6	0.6	0.0558	0.0580	0.0084	37.3	37.4	0.3
2024	-1308	-1333	762	1.9	2.3	1.6	22.8	22.6	0.9	0.0658	0.0726	0.0227	37.4	37.4	0.5
2025	-1276	-1270	764	1.9	2.3	1.6	25.2	25.2	1.2	0.0574	0.0594	0.0106	37.3	37.3	0.4
2010-2025	-1179	-1228	776	2.0	2.3	1.6	23.3	23.3	1.8	0.0598	0.0658	0.0486	37.4	37.4	
	GradSpat_SST			**GradSpat_SS**			**SST7dinc**			**SST15dinc**			**CHL7d_mean**		
Year	**median**	**mean**	**sd**	**median**	**mean**	**sd**	**median**	**mean**	**sd**	**median**	**mean**	**sd**	**median**	**mean**	**sd**
2010	1.3	1.5	0.8	0.7	0.8	0.5	1.2	1.2	1.0	2.4	2.1	1.6	0.1	0.1	0.0
2013	1.7	1.8	1.0	0.9	1.1	0.8	0.8	1.0	0.8	1.9	2.0	1.0	0.1	0.1	0.1
2015	1.3	1.5	0.7	0.9	1.2	0.8	1.5	1.5	0.3	2.0	2.0	0.4	0.0	0.1	0.0
2017	1.4	1.6	0.8	1.1	1.3	0.7	1.4	1.4	0.9	2.4	2.4	0.8	0.1	0.1	0.0
2018	1.3	1.6	0.9	0.8	0.9	0.6	1.2	1.2	0.7	2.5	2.5	0.7	0.1	0.1	0.0
2019	2.1	2.1	1.1	1.1	1.3	0.7	1.1	1.2	0.6	2.0	2.1	0.6	0.1	0.1	0.0
2022	1.5	1.7	0.8	0.8	0.9	0.6	1.1	1.0	1.1	2.6	2.5	1.4	0.1	0.1	0.0
2023	1.2	1.2	0.6	1.2	1.3	0.6	1.8	1.8	0.6	2.9	2.9	0.9	0.1	0.1	0.0
2024	1.3	1.4	0.7	1.5	1.7	1.1	1.0	0.9	0.9	1.5	1.4	0.8	0.1	0.1	0.0
2025	1.2	1.3	0.7	1.4	1.5	0.7	1.4	1.4	0.6	2.8	2.9	0.5	0.1	0.1	0.0
2010-2025	1.3	1.5	0.8	1.0	1.2	0.8	1.3	1.2	0.9	2.4	2.3	1.1	0.0611	0.0665	

Spatial gradient of sea surface temperature (GradSpat_SST)

The mean spatial gradient of sea surface temperature (GradSpat_SST) in the segment's MidLon-MidLat locations was 1.5 ºC (± 0.8 SD; Table 2.6). Annual variability shows median values generally around 1.3 ºC (Figure 2.23), with the year 2019 showing slightly higher median value, around 2ºC.

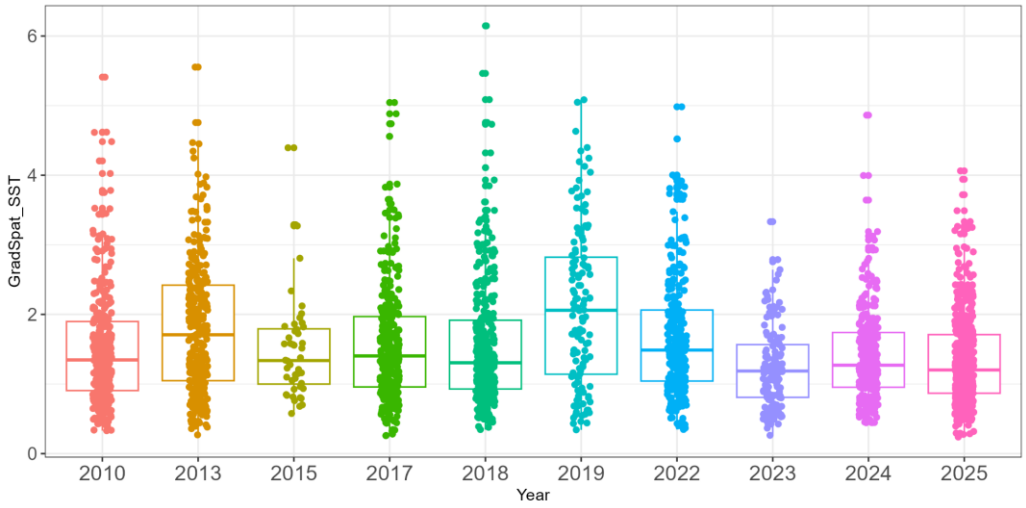

Figure 2.23. Spatial gradient of sea surface temperature (GradSpat_SST, ºC): environmental variability in the aerial survey sampling segments for the period 2010-2025.

Spatial gradient of sea surface salinity (GradSpat_SSS)

The mean spatial gradient of sea surface salinity (GradSpat_SSS) in the segment's MidLon-MidLat locations was 1.2 (± 0.8 SD; Table 2.6). Annual variability shows median values around 1.0, with the latter years (2022 to 2025) seemingly showing higher median values, suggesting a possible increasing trend (Figure 2.24, Table 2.6). This result should be considered in the process of standardization, as inter-annual trends of relevant variables included in standardization models can mask trends in abundance.

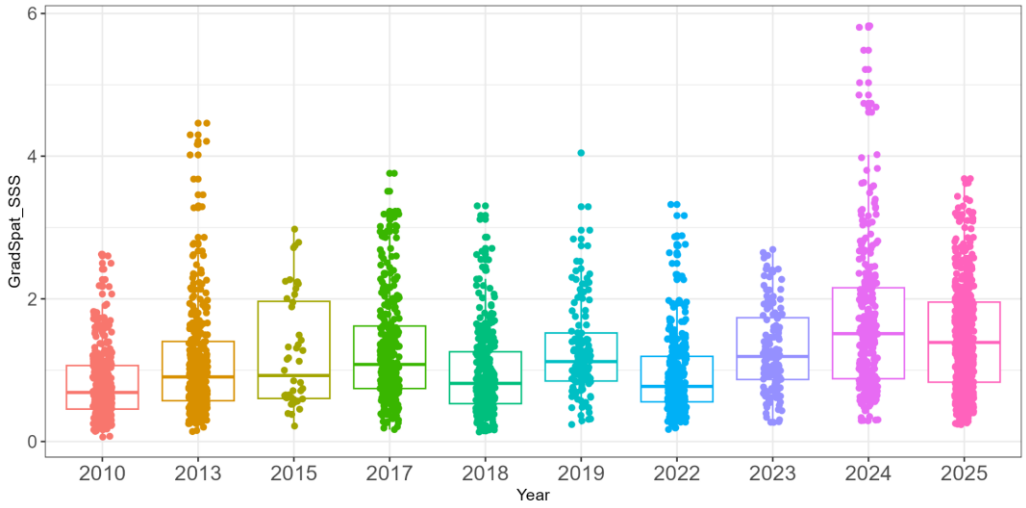

Figure 2.24. Spatial gradient of sea surface salinity (GradSpat_SST, ºC): environmental variability in the aerial survey sampling segments for the period 2010-2025.

Seven-day increase in sea surface temperature (SST7d_inc)

The seven-day increase in sea surface temperature (SST7d_inc) in the segment's MidLon-MidLat locations from the aerial surveys was 1.2 ºC (± 0.9 SD; Table 2.6). Annual variability shows median values around 1.3 ºC, with some years like 2015, 2023 and 2025 showing slightly higher median values (Figure 2.25, Table 2.6). No general trend is observed.

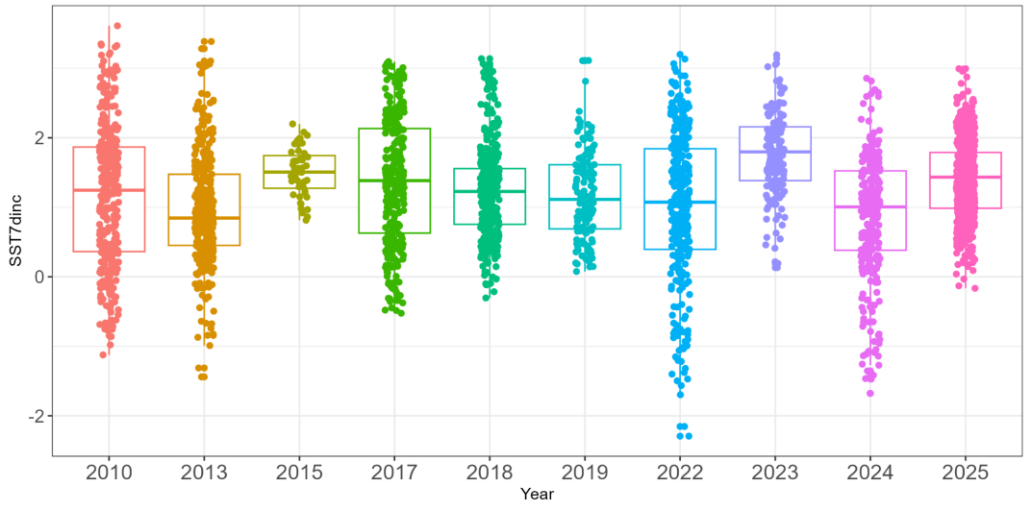

Figure 2.25. Seven-day increase in sea surface temperature (SST7d_inc, ºC): environmental variability in the aerial survey sampling segments for the period 2010-2025.

Fifteen-day increase in sea surface temperature (SST15d_inc)

The fifteen-day increase in sea surface temperature (SST15d_inc) was 2.3 ºC (± 1.1 SD; Table 2.6). Annual variability shows median values around 2.4 ºC (Figure 2.26, Table 2.6). There are some years with high intra-annual variability (2010, 2013, 2022) which should be investigated.

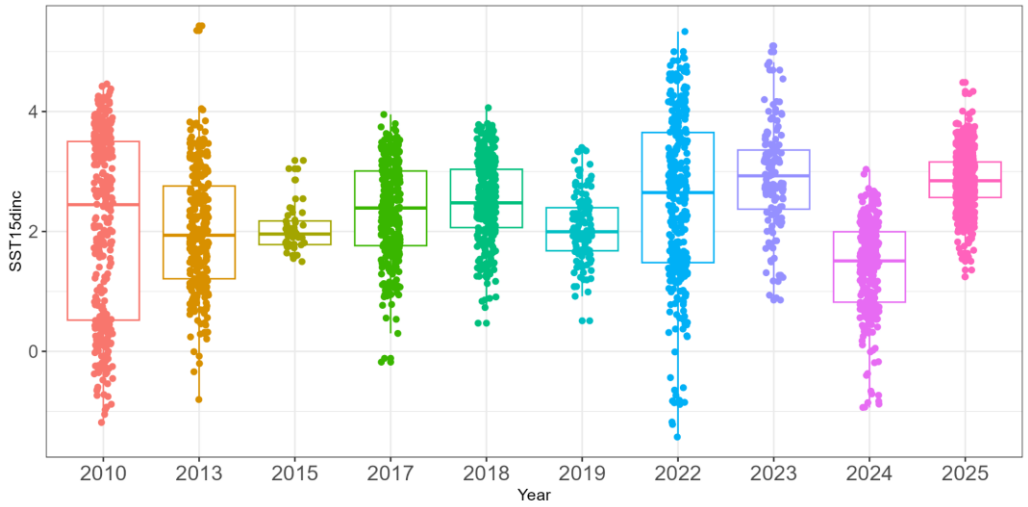

Figure 2.26. Fifteen day increase in sea surface temperature (SST7d_inc, ºC): environmental variability in the aerial survey sampling segments for the period 2010-2025.

Multidimensional analysis

Results from the principal component analysis (PCA) of environmental variables at the segment level are presented in Figure 2.28. The analysis is shown for individual segments and grouped by year. The first two principal components explain approximately 46–47% of the total standardised environmental variance. This indicates that a substantial fraction of the environmental variability observed during the surveys can be represented in a two-dimensional space. PCA scatterplots show that observations from different years occupy partially overlapping, but also distinct, regions of the environmental space. Annual centroids are separated along both PC1 and PC2, indicating that each survey year is characterised by a specific combination of environmental conditions.

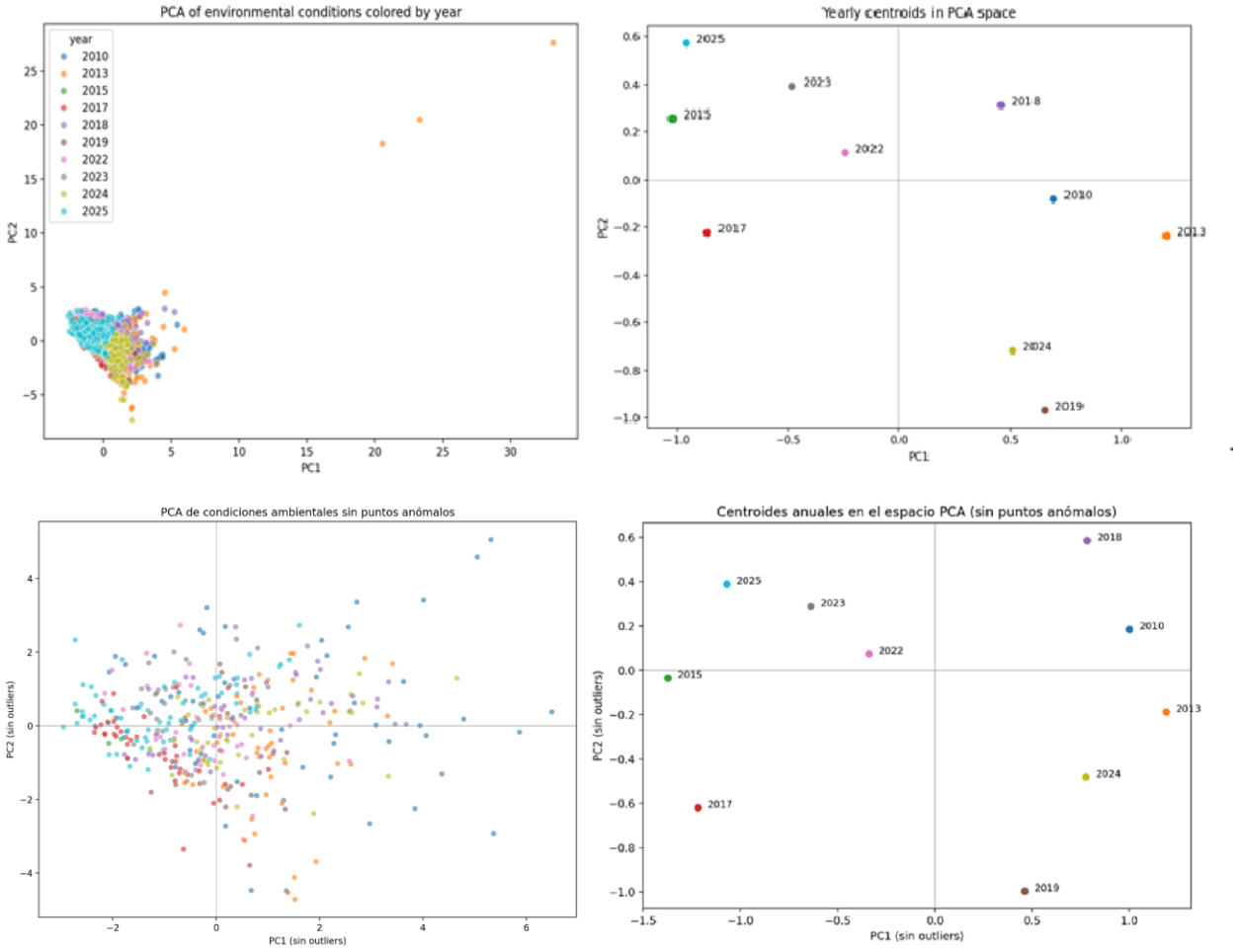

Figure 2.28. PCA of the segments (left) and by years (right): for all the dataset (upper panel) and after removing outliers (lower panel).

The yearly analysis, show that some years are clustered closely together (right plots in Figure 2.28), reflects similar environmental backgrounds, whereas other years were clearly offset, suggesting environmentally distinct survey conditions of two groups of years (2015, 2017, 2022, 2023, 2025 and 2010, 2013, 2018, 2019, 2024).

By combining the PCA results with univariate summaries of environmental variables (boxplot figures from segment data), the main drivers of inter-annual separation can be summarised as follows:

1) The relation between sea surface temperature and mixed layer depth tends to group together the different years.
2) Years characterised by stronger SST gradients or larger short-term SST changes were associated with more frontal or transitional conditions.
3) Years with higher chlorophyll concentrations were environmentally distinct in terms of productivity.

Differences in the distribution of sampling day-of-year among years contributed to the observed inter-annual separation in PCA space. Years sampled earlier in the season tended to appear cooler and more mixed, whereas years sampled later were characterised by warmer, more stratified conditions.

Only a small number of observations were classified as extreme in PCA space. After removing these points and recomputing the PCA, the overall structure of the environmental space and the relative separation of annual centroids remained consistent. This indicates that the observed inter-annual patterns are robust and not driven by a few anomalous observations.

Nevertheless, these anomalous observations can cause strong effects in statistical models, and it is suggested not to include them in the modelling phase.

2.4. Discussion

In this study, environmental variability characterising the Atlantic Bluefin tuna spawning area in the Balearic Sea during the GBYP aerial survey sampling period has been analysed in an integrated manner, considering both a broad spatial scale representative of the recurrently sampled spawning area and the specific scale of the segments (20km length) derived from flight transects. This multiscale approach has made it possible to assess the extent to which the oceanographic conditions observed during flights are comparable among years and, consequently, to identify potential sources of non-biological variability that may influence the interpretation of abundance indices derived from aerial censuses.

The results show clear and consistent inter-annual environmental differences, both at the scale of the study area and at the level of the sampling segments, affecting key variables related to the structure of the Bluefin tuna spawning habitat. At the area scale, marked inter-annual variability is observed in sea surface temperature, salinity, and the relative position of fronts associated with the confluence of recent Atlantic waters and resident Mediterranean waters, together with

a significant trend towards an earlier time of year at which the 20 °C thermal threshold—commonly associated with the onset of reproductive activity—is exceeded. This advance, estimated at approximately half a day per year, has direct implications for the synchronisation between the survey period and the reproductive phenology of the stock.

At the segment scale, the results reveal considerable environmental heterogeneity among years and within each survey, with systematic differences in temperature, salinity, spatial gradients associated with frontal structures, and short-term thermal variability metrics. Multivariate analysis confirms that each sampling year occupies a partially differentiated region of the environmental space, reflecting specific combinations of oceanographic conditions during the flights. This persistent inter-annual structure indicates that aerial surveys are not conducted under a homogeneous environmental context, reinforcing the need to interpret observed variations in abundance indices in light of spawning habitat variability. Overall, these results suggest that a fraction of the inter-annual variability in encounter rates may be associated with shifts and changes in the location of the spawning habitat, rather than with genuine fluctuations in the biomass of the spawning stock.

From the perspective of analysing the variables individually, it should be borne in mind that certain variables, such as salinity and mixed layer depth, are products derived from hydrodynamic models rather than from in situ observations. From these data sets we show inter-annual fluctuations around the Balearic Islands (37.5 psu) what has been previously documented from in-situ data (Balbín et al., 2014). However, a recent study suggests that this front is shifting northwards (Camps, 2025), what could have relevant implications on the spatial distribution of the spawning aggregations. Although, in the regional (area-based) analysis—whether in the boxplots, line plots or even in the annual maps (see Figure 2.8, Annex 1.3)—the environmental data extracted at the mid-location of the aerial survey segments (MidLon, MidLat) appear to show a certain reduction in sea surface salinity (SSS), suggesting a greater coverage of less saline Atlantic waters. This pattern is consistent with the northward displacement mentioned above.

The day on which sea surface temperature (SST) exceeds 20 °C in the spawning area is advancing at a rate of approximately 0.5 days per year; therefore, caution is required when designing the sampling surveys, as spawning aggregations may form earlier and fish may abandon the area also earlier. Chlorophyll-a (CHL) exhibits highly localised peaks in concentration, both in time and space, which are smoothed in the weekly averages, although they remain detectable. This behavior is inherent to the nature of this variable; however, it may occasionally lead to reduced predictive performance in the models, excluding out layers in the standardizations models should be considered.

2.5. Conclusions and considerations for the future standardization of abundance indices from aerial surveys

1- Potential relevance of environmental effects in the calculation of abundance indices. The marked inter-annual structure of the environmental space suggest that the observed changes in abundance indices may reflect variability in the spawning habitat rather than genuine fluctuations in spawning biomass. Standardisation models should therefore explicitly distinguish between environmental signals and demographic signals.

2- Systematic incorporation of relevant environmental covariates
Variables such as sea surface temperature, salinity, spatial gradients associated with fronts, and short-term thermal variability metrics have shown significant inter-annual variability and clear ecological relevance. Their inclusion in standardisation models is essential to reduce biases associated with changes in sampling conditions. Within these models, marginalization of environmental covariates should be incorporated, which refers to the process of obtaining predictions or estimates by averaging model outputs over a specified distribution of covariates, thereby isolating the effect of the focal variable of interest (e.g. year) from other sources of variability.

3- Explicit treatment of seasonality and reproductive phenology
The progressive advance in the timing at which the 20 °C thermal threshold is reached suggests a possible shift in reproductive phenology. Models should consider temporal variables (day of year, thermal phase, or phenological proxies) in order to avoid confounding changes in the sampling calendar with changes in abundance.

4- Consideration of the appropriate spatial scale for modelling
The environmental variability observed at the segment scale highlights that the spatial scale of analysis directly influences the ability to detect ecological relationships. The selection of spatial resolution should be carefully evaluated during the modelling phase to balance ecological realism and statistical stability. This is closely linked to the effect of transect length on the proportion of zero observations in abundance data, which can substantially constrain the choice of standardisation methodologies. For these reasons, it is recommended to assess the feasibility and potential benefits of increasing transect length to 40 or 60 km, which could increase the number of transects with positive observations without an overly substantial loss of environmental information associated with each transect.

5- Critical evaluation of the use of model-derived variables
Variables such as mixed layer depth or certain salinity products, being derived from hydrodynamic models, should be interpreted with caution. Their inclusion in standardisation models should be accompanied by sensitivity analyses and, where possible, cross-validation with independent observations.

6- Identification and treatment of environmentally extreme observations
Multivariate analysis has identified a small number of segments with extreme environmental combinations. Although they do not alter the overall structure of the environmental space, these observations may have a disproportionate influence on models and should therefore be explicitly evaluated (inclusion/exclusion) during standardisation.

7- Specific assessment of environmentally contrasted years
Some years exhibit clearly differentiated environmental configurations. These years should be analysed explicitly within standardisation models to assess whether anomalies in the indices persist once environmental and seasonal effects are controlled for.

8- Need for a multivariate and reproducible approach
The complexity and covariation of environmental variables justify the use of multivariate approaches (e.g. spatial models, GAMs, GLMMs or synthetic components such as PCA), within a transparent and reproducible methodological framework that is coherent with subsequent application in ICCAT MSE processes.

ACKNOWLEDGEMENTS

This work was carried out under the provision of the ICCAT. The contents of this document do not necessarily reflect the point of view of ICCAT, which has no responsibility over them, and in no ways anticipate the Commission's future policy in this area. This work was conducted within the ICCAT Atlantic-Wide Research Programme for Bluefin Tuna (GBYP) and partially funded by the European Union through the EU Grant Agreement No. 101169569 - GBYP Phase 14.. MP Tugores participated in this document as a member of the TUNAWAVE project, within the project work package devoted to Transference. We also acknowledge the Mediterranean Tuna Habitat initiative (TunaMed, https://oostop.wixsite.com/tunamed) for the inputs and feedback on identification of habitat indicators of interest for this work.

REFERENCES

Alemany, F., L. Quintanilla, P. Vélez-Belchí, A. García, D. Cortés, J. M. Rodríguez, M. F. de Puelles, C. González-Pola, and J. L. López-Jurado. 2010. Characterization of the spawning habitat of Atlantic bluefin tuna and related species in the Balearic Sea (western Mediterranean). Progress in Oceanography **86**:21-38.

Alvarez-Berastegui, D., L. Ciannelli, A. Aparicio-Gonzalez, P. Reglero, M. Hidalgo, J. L. López-Jurado, J. Tintoré, and F. Alemany. 2014. Spatial scale, means and gradients of hydrographic variables define pelagic seascapes of bluefin and bullet tuna spawning distribution. PLoS ONE **9**:e109338.

Alvarez-Berastegui, D., M. Hidalgo, M. P. Tugores, P. Reglero, A. Aparicio-González, L. Ciannelli, M. Juza, B. Mourre, A. Pascual, and J. L. López-Jurado. 2016. Pelagic seascape ecology for operational fisheries oceanography: modelling and predicting spawning distribution of Atlantic bluefin tuna in Western Mediterranean. ICES Journal of Marine Science **73**:1851-1862.

Aranda, G., F. J. Abascal, J. L. Varela, and A. Medina. 2013. Spawning behaviour and post-spawning migration patterns of Atlantic bluefin tuna (*Thunnus thynnus*) ascertained from satellite archival tags. PLoS ONE **8**: e76445.

Bakun A. 2006. Fronts and eddies as key structures in the habitat of marine fish larvae: opportunity, adaptive response and competitive advantage. Sci Mar, 71 (S2): 105-122 https://doi.org/10.3989/scimar.2006.70s2105

Balbín, R., J. L. López-Jurado, M. d. M. Flexas, P. Reglero, P. Vélez-Velchí, C. González-Pola, J. M. Rodríguez, A. García, and F. Alemany. 2014. Inter-annual variability of the early summer circulation around the Balearic Islands: driving factors and potential effects on the marine ecosystem. Journal of Marine Systems **138**:70-81.

Bettencourt, J. H., C. López, and E. Hernández-García. 2012. Oceanic three-dimensional Lagrangian coherent structures: A study of a mesoscale eddy in the Benguela upwelling region. Ocean Modelling **51**:73-83.

Block, B. A., S. L. Teo, A. Walli, A. Boustany, M. J. Stokesbury, C. J. Farwell, K. C. Weng, H. Dewar, and T. D. Williams. 2005. Electronic tagging and population structure of Atlantic bluefin tuna. Nature **434**:1121-1127.

Buckland, S. T., D. R. Anderson, K. P. Burnham, J. L. Laake, D. L. Borchers, and L. Thomas. 2001. Introduction to Distance Sampling. Estimating abundance of biological populations. Oxford University Press, Oxford.

Burden, R. L., Faires, J. D. 2005. Numerical Analysis (8th ed.). Brooks/Cole, Cengage Learning. 847 pp.

Camps, M. 2025. Summer surface circulation around the Balearic Islands: model and data indicators of a northward trend of the salinity front, Master's Degree in Advanced Physics and Applied Mathematics, Centre for Postgraduate Studies, Universitat de les Illes Balears.

Cornic M, Rooker JR. 2018. Influence of oceanographic conditions on the distribution and abundance of blackfin tuna (*Thunnus atlanticus*) larvae in the Gulf of Mexico. Fish Res, 201: 1-10. https://doi.org/10.1016/j.fishres.2017.12.015

Díaz-Barroso, L., I. Hernández-Carrasco, A. Orfila, P. Reglero, R. Balbín, M. Hidalgo, J. Tintoré, F. Alemany, and D. Álvarez-Berastegui. 2022. Singularities of surface mixing activity in the Western Mediterranean influence bluefin tuna larval habitats. Marine Ecology Progress Series **685**:69-84.

Di Natale, A., Tensek, S. & Pagá García, A. (2015). 2015: Is the bluefin tuna facing another 2003?. SCRS/2015/154, Collect. Vol. Sci. Pap. ICCAT 72(6): 1614–1630.

Fujioka, K., Hiraoka, Y., Kuwahara, T., Tsukahara, Y., & Fukuda, H. (2025). Post-spawning migration and habitat use of adult Pacific bluefin tuna (*Thunnus orientalis*) in the western North Pacific. Marine Biology. https://doi.org/10.1007/s00227-025-04596-6

Fujioka, K., Sasagawa, K., Kuwahara, T., Takahara, Y., Komeyama, K., Kitagawa, T., Farwell, C., Furukawa, S., Kinoshita, J., Fukuda, H., Kato, M., Aoki, A., Abe, O., Ohshimo, S., & Suzuki, N. (2021). Habitat use of adult Pacific bluefin tuna *Thunnus orientalis* during the spawning season in the Sea of Japan: evidence for a trade-off between thermal preference and reproductive activity. Marine Ecology Progress Series **668**: 1-20. https://doi.org/10.3354/meps13746

García, A., F. Alemany, P. Vélez-Belchí, J. L. López Jurado, D. Cortés, J. De la Serna, C. González Pola, J. Rodríguez, J. Jansá, and T. Ramírez. 2005. Characterization of the bluefin tuna spawning habitat off the Balearic Archipelago in relation to key hydrographic features and associated environmental conditions. Col. Vol. Sci. Pap. ICCAT **58**:535-549.

Gonzalez, R. C., Woods, R. E. 2018. Digital Image Processing (4th ed.). Pearson. 1168 pp.

Gordoa, A., Carreras G. 2014. Determination of temporal spawning patterns and hatching time in response to temperature of Atlantic bluefin tuna (*Thunnus thynnus*) in the Western Mediterranean. PLoS ONE **9**: e90691.

Grolemund G, Wickham H. 2011. Dates and Times Made Easy with lubridate. Journal of Statistical Software, 40(3), 1-25. URL https://www.jstatsoft.org/v40/i03/

Gille ST, Metzger EJ, Tokmakian R. 2003. Seafloor Topography and Ocean Circulation. Oceanography, 17 (1): 47-54Glover DM, Brewer PG. 1988: Estimates of wintertime mixed layer nutrient concentrations in the North Atlantic. Deep-Sea Res, 35: 1525-1546 https://doi.org/10.1016/0198-0149(88)90101-X

Hazen, E. L., A. B. Carlisle, S. G. Wilson, J. E. Ganong, M. R. Castleton, R. J. Schallert, M. J. Stokesbury, S. J. Bograd, and B. A. Block. 2016. Quantifying overlap between the Deepwater Horizon oil spill and predicted bluefin tuna spawning habitat in the Gulf of Mexico. Scientific Reports **6**:33824.

Hedley, S. L., and S. T. Buckland. 2004. Spatial models for line transect sampling. Journal of Agricultural, Biological, and Environmental Statistics **9**:181-199.

Hernández-Carrasco, I., C. López, E. Hernández-García, and A. Turiel. 2011. How reliable are finite-size Lyapunov exponents for the assessment of ocean dynamics? Ocean Modelling **36**:208-218.

Hijmans, R. J. 2023a. raster: Geographic data analysis and modeling. R package version 3.6-26. https://CRAN.R-project.org/package=raster

Hijmans, R. J. 2023b. terra: Spatial Data Analysis. R package version 1.7-65. https://CRAN.R-project.org/package=terra

Horn, B.K.P. 1981. Hill shading and the reflectance map. Proceedings of the IEEE 69:14-47

ICCAT. 2011. Report of the 2011 ICCAT Bluefin Tuna Atlantic-Wide Research Programme (GBYP) Aerial Survey. ICCAT SCRS/2011/145. ICCAT, Madrid.

ICCAT. 2021. Report of the 2021 ICCAT Bluefin Tuna Stock Assessment Session. ICCAT Annual Report, Vol. 2. ICCAT, Madrid.

Juza, M., Tintoré, J. 2021. Multivariate Sub-Regional Ocean Indicators in the Mediterranean Sea: From Event Detection to Climate Change Estimations. Frontiers in Marine Science, 8, 610589. https://doi.org/10.3389/fmars.2021.610589

Koched, W., A. Hattour, F. Alemany, and A. García-García. 2013. Spatial distribution of tuna larvae in the Gulf of Gabes (Eastern Mediterranean) in relation with environmental parameters. Mediterranean Marine Science **14**:5-14.

Laake, J., D. Borchers, L. Thomas, D. Miller, and J. Bishop. 2022. mrds: mark–recapture distance sampling. R package version 2.2.8. https://cran.r-project.org/package=mrds.

Llopiz, J. K., and A. J. Hobday. 2015. A global comparative analysis of the feeding dynamics and environmental conditions of larval tunas, mackerels, and billfishes. Deep Sea Research Part II: Topical Studies in Oceanography **113**:113-124.

Marques, T. A., L. Thomas, S. G. Fancy, and S. T. Buckland. 2007. Improving estimates of bird density using multiple-covariate distance sampling. The Auk **124**:1229-1243.

Marcek, B., Fabrizio, M., & Graves, J. 2016. Short-Term Habitat Use of Juvenile Atlantic Bluefin Tuna. Marine and Coastal Fisheries: Dynamics, Management, and Ecosystem Science **8**: 395-403. https://doi.org/10.1080/19425120.2016.1168330

Marshall D. 1995. Influence of topography on the large-scale ocean circulation. Journal of Physical Oceanography **25**: 1622-1635.

Medina, A., F. Abascal, C. Megina, and A. Garcia. 2002. Stereological assessment of the reproductive status of female Atlantic northern bluefin tuna during migration to Mediterranean spawning grounds through the Strait of Gibraltar. Journal of Fish Biology **60**:203-217.

Muhling, B. A., S.-K. Lee, J. T. Lamkin, and Y. Liu. 2011. Predicting the effects of climate change on bluefin tuna (*Thunnus thynnus*) spawning habitat in the Gulf of Mexico. ICES Journal of Marine Science **68**: 1051-1062.

Muhling, B. A., P. Reglero, L. Ciannelli, D. Alvarez-Berastegui, F. Alemany, J. T. Lamkin, and M. A. Roffer. 2013. Comparison between environmental characteristics of larval bluefin tuna *Thunnus thynnus* habitat in the Gulf of Mexico and western Mediterranean Sea. Marine Ecology Progress Series **486**:257-276.

Ottmann D, Fiksen Ø, Martín M, Alemany F, Prieto L. 2021. Spawning site distribution of a bluefin tuna reduces jellyfish predation on early life stages. Limnol Oceanogr, 66: 3669–3681 https://doi.org/10.1002/lno.11908

Paxton, C. G. M., Oedekoven, C., Burt, L., Chudzińska, M., Tugores Ferrà, M. P., Álvarez-Berastegui, D. 2023. Design- and model-based inference to estimate density, abundance and distribution of bluefin tuna in the Mediterranean Sea. CREEM Report 2023-04. Provided to ICCAT.

Pebesma, E., and R. Bivand. 2023. Spatial data science: With applications in R. CRC Press.

Pierce, D. 2023. ncdf4: Interface to Unidata netCDF (Version 4 or Earlier) Format Data Files. R package version 1.22, https://CRAN.R-project.org/package=ncdf4

R Core Team. 2024. R: A language to environment for statistical computing. R Foundation for Statistical Computing, Vienna, Austria, URL https://www.R-project.org/.

R Core Team. 2023. R: A language to environment for statistical computing. R Foundation for Statistical Computing, Vienna, Austria, URL https://www.R-project.org/.

Reglero, P., L. Ciannelli, D. Álvarez-Berastegui, R. Balbín, J. L. López-Jurado, and F. Alemany. 2012. Geographically and environmentally driven spawning distributions of tuna species in the western Mediterranean Sea. Marine Ecology Progress Series **463**:273-284.

Reglero, P., D. P. Tittensor, D. Álvarez-Berastegui, A. Aparicio-González, and B. Worm. 2014. Worldwide distributions of tuna larvae: revisiting hypotheses on environmental requirements for spawning habitats. Marine Ecology Progress Series **501**:207-224.

Rosselló, P., Pascual, A., Combes, V. 2023. Assessing marine heat waves in the Mediterranean Sea: a comparison of fixed and moving baseline methods. Frontiers in Marine Science, 10, 1168368. https://doi.org/10.3389/fmars.2023.1168368

Solodoch A. 2020. Topographic effects on mesoscale ocean circulation. Thesis Dissertation, PhD Atmospheric and Oceanic Sciences, University of California, 237 pp.

Suthers IM, Schaeffer A, Archer M, Roughan M, Griffin DA, Chapman CC, Sloyan BM, Everett JD. 2023. Frontal eddies provide an oceanographic triad for favorable larval fish habitat. Limnol Oceanogr, 68: 1019–1036 https://doi.org/10.1002/lno.12326

Tintoré, J., Lana, A., Marmain, J., Fernández, V., Casas, B., & Reyes, E. (2020). HF Radar Ibiza data from date 2012-06-01 (Version 1.0.2) [Data set]. Balearic Islands Coastal Observing and Forecasting System, SOCIB. https://doi.org/10.25704/17GS-2B59

Trueman, C., Artetxe-Arrate, I., Kerr, L., Meijers, A., Rooker, J., Sivankutty, R., Arrizabalaga, H., Belmonte, A., Deguara, S., Goñi, N., Rodriguez-Marin, E., Dettman, D., Santos, M., Karakulak, F., Tinti, F., Tsukahara, Y., & Fraile, I. 2023. Thermal sensitivity of field metabolic rate predicts differential futures for bluefin tuna juveniles across the Atlantic Ocean. Nature Communications **14:** https://doi.org/10.1038/s41467-023-41930-2

Volpe, G., Colella, S., Brando, V. E., Forneris, V., Padula, F. L., Cicco, A. D., ... & Santoleri, R. (2019). Mediterranean ocean colour Level 3 operational multi-sensor processing. Ocean Science **15**(1): 127-146

Walter, J., Rouyer, T., & Kimoto, A. 2025. Informal summary of the 2025 ICCAT Bluefin Tuna Species Group Meeting (24–26 September 2025). Collective Volume of Scientific Papers ICCAT **82**(4), SCRS/2025/239: 1–20.

Worm, B., M. Sandow, A. Oschlies, H. K. Lotze, and R. A. Myers. 2005. Global patterns of predator diversity in the open oceans. Science **309**:1365-1369.

Appendix A. Summary of school sizes, biomass and perpendicular distances by year

This appendix summarises key information needed for each BFT school by year: school size, total biomass and the perpendicular distance. Table A1 contains the median of these values and Figure A1 shows the distributions. Note that these values include juvenile schools and schools detected beyond 1,500m.

Table A1. Number of all detected schools of BFT on search effort along the transects in block A and median values of school size, biomass and perpendicular distance.

Year	Number of schools	Median school size (individuals)	Median biomass (kg)	Median perpendicular distance (m)
2017	21	7	1,170	187
2018	27	700	106,000	151
2019	12	325	50,000	511
2021	9	935	180,000	427
2022	19	980	165,000	1,192
2023	34	625	77,500	288
2024	11	30	750	373
2025	18	70	1,400	405

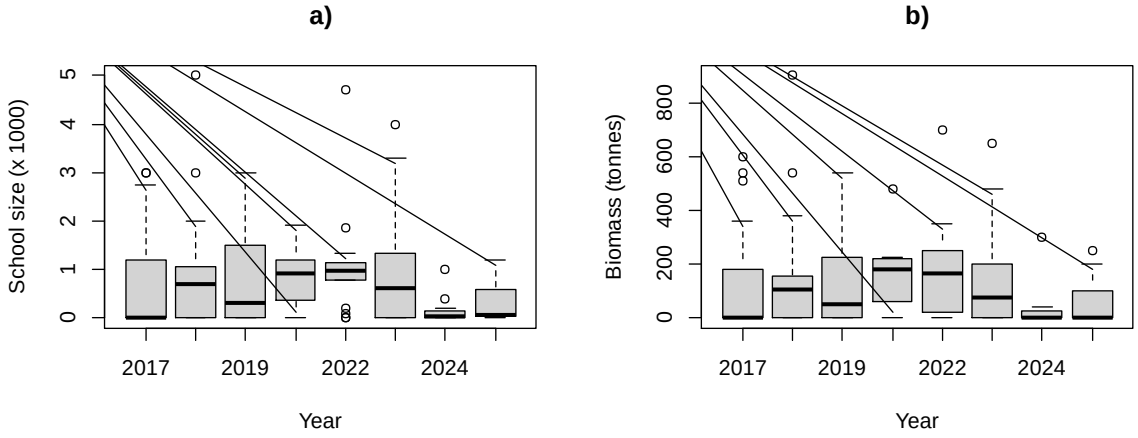

Figure A1. Distributions of BFT school sizes and biomass recorded by year in block A. It includes all schools, including juveniles, and the sightings have not been truncated. The thick black line on each 'box' indicates the median, and the upper and lower limits of the box indicate the interquartile range (IQR), the whiskers extend to, at most, 1.5 times the IQR from the box and points outside this (circles) indicate extreme values.

Appendix B. Calculating perpendicular distance

The perpendicular distance from the detected school to the transect was calculated using the trigonometric relationship:

$$y_i = h_i * \tan((90 - \theta_i)$$

where y_i is the perpendicular distance between the transect and the i^{th} school, θ_i is the declination angle measured when the plane was a beam and h_i is the height of the airplane above sea level when abeam of the detected school.

Appendix C. Detection function selection

Table C1. AIC values from fitting detection functions with different key functions and covariates. 'None' indicates that a conventional distance sampling function was fitted. Bold indicates the selected model.

Covariates	Half-normal	Hazard rate
Log(size)	**1518.6**	1526.6
Log(size) + Company	1521.3	1526.3
Log(biomass)	1539.5	1541.8
Year (factor with 8 levels)	1574.5	1553.0
None	1583.7	1562.4
Company (factor with 3 levels)	1587.0	1564.4

Appendix D. Spatio-temporal variability in sea surface temperature (SST) across the aerial survey timeframe (28 May–11 July) from 2010 to 2025

See separate file: “Appendix_D_SpatTemp_Yearly_Maps_SST.docx”

Appendix E. Spatio-temporal variability in sea surface chlorophyll-a (CHL) across the aerial survey timeframe (28 May–11 July) from 2010 to 2025

See separate file: “Appendix_E_SpatTemp_Yearly_Maps_CHL.docx”

Appendix F. Spatio-temporal variability in sea surface salinity (SSS) across the aerial survey timeframe (28 May–11 July) from 2010 to 2025

See separate file: “Appendix_F_SpatTemp_Yearly_Maps_SST.docx”

Appendix G. Spatio-temporal variability in sea surface mixed layer depth (MLD) across the aerial survey timeframe (28 May–11 July) from 2010 to 2025

See separate file: “Appendix_G_SpatTemp_Yearly_Maps_MLD.docx”

Appendix H. Spatio-temporal variability in spatial gradient of sea surface temperature (GradSpat SST) across the aerial survey timeframe (28 May–11 July) from 2010 to 2025

See separate file: “Appendix_H_SpatTemp_Yearly_Maps_GradSpat_SST.docx”

Appendix E. Spatio-temporal variability in spatial gradient of sea surface salinity (GradSpat SSS) across the aerial survey timeframe (28 May–11 July) from 2010 to 2025

See separate file: “Appendix_E_SpatTemp_Yearly_Maps_GradSpat_SSS.docx”